JBC RESEARCH ARTICLE

Scalable purification enables high-quality virus-like particles for therapeutic translation

Received for publication, September 23, 2025, and in revised form, November 3, 2025 Published, Papers in Press, November 13, 2025
https://doi.org/10.1016/j.jbc.2025.110946

Rafal Hołubowicz[1,*], Fangyuan Gao[1], Samuel W. Du[1,2], Carolline Rodrigues Menezes[1,2], Jianye Zhang[1], Maria W. Hołubowicz[1], Paul Z. Chen[3,4,5,6], Niklas Armbrust[7,8], Julian Geilenkeuser[7,8], David R. Liu[3,4,5], Dong-Jiunn Jeffery Truong[7,8], Gil Gregor Westmeyer[7,8], Grazyna Palczewska[1], and Krzysztof Palczewski[1,2,9,10,*]

From the [1]Gavin Herbert Eye Institute –Brunson Center for Translational Vision Research, Department of Ophthalmology and Visual Sciences, University of California Irvine, Irvine, California, USA; [2]Department of Physiology and Biophysics, University of California Irvine, Irvine, California, USA; [3]Merkin Institute of Transformative Technologies in Healthcare, Broad Institute of MIT and Harvard, Cambridge, Massachusetts, USA; [4]Department of Chemistry and Chemical Biology, Harvard University, Cambridge, Massachusetts, USA; [5]Howard Hughes Medical Institute, Harvard University, Cambridge, Massachusetts, USA; [6]David H. Koch Institute for Integrative Cancer Research, Massachusetts Institute of Technology, Cambridge, Massachusetts, USA; [7]Institute for Synthetic Biomedicine, Helmholtz Munich, Neuherberg, Germany; [8]Department of Bioscience, TUM School of Natural Sciences, Technical University of Munich, Munich, Germany; [9]Department of Chemistry, University of California Irvine, Irvine, California, USA; [10]Department of Molecular Biology and Biochemistry, University of California Irvine, Irvine, California, USA

Reviewed by members of the JBC Editorial Board. Edited by Kirill Martemyanov

Emerging molecular therapies introduce enzymatic activity into cells by delivering genes, transcripts, or proteins. Owing to their robust cell-entry capacity, virus-like particles (VLPs) represent a technology of choice in genome editing, where low doses of heterologous proteins and nucleic acids are essential. However, clinical translation of VLP vectors is hindered by inadequate purification methods. Current approaches, relying primarily on ultracentrifugation, suffer from inconsistent product quality and poor scalability. Here, we report the development of a broadly applicable purification strategy that improves the purity and therapeutic efficacy of genome-editing VLPs. Considering the characteristic properties of murine leukemia virus-derived engineered VLPs and HIV-derived engineered nucleocytosolic vehicles for loading of programmable editors, we developed a workflow that involves single-modal and multimodal chromatographic steps, effectively removing host cell proteins and cell-culture contaminants while improving VLP integrity and biological activity. Our purified VLPs displayed superior protein composition, consistency, and enhanced functional delivery compared to VLPs partially purified by conventional ultracentrifugation methods. Mass spectrometric analysis revealed a substantial decrease in contaminants, with VLP-specific proteins comprising >90% of the final product. *In vivo* studies confirmed improved therapeutic outcomes when chromatographically purified VLPs were used. Our scalable purification platform addresses critical manufacturing bottlenecks and constitutes a starting point for further development of VLP therapeutics, enabling robust production of pure VLPs for diverse applications such as genome editing, vaccine development, and other uses that require intracellular protein delivery.

Genome editing is a rapidly evolving field of translational research. CRISPR-Cas proteins, which are often complemented by the activities of the fused enzymes DNA deaminase (base editing, BE) or reverse transcriptase (prime editing, PE), with their specific guide RNAs, introduce preprogrammed changes into the genome (1–4). Thus, it is now possible to cure disabling genetic disorders that were previously untreatable. The ability to program BE and PE to modify a specific disease-causing variant by merely changing the sequence of the guide RNA makes it possible to tailor genome-editing therapies to individual patients (5–7). However, the lack of appropriate ribonucleoprotein (RNP) delivery techniques poses an obstacle to the application of these life-saving therapies. Genome-editing therapy requires intracellular delivery of proteins; therefore, implementation can be challenging due to poor tissue permeability, immune-clearance mechanisms, inefficient endosomal escape, and/or proteolytic degradation (8–11).

The use of viral vectors is a well-established way to express heterologous proteins *in vivo*. Adeno-associated virus (AAV), the most commonly used, as well as adenovirus and lentivirus, have genomes amenable to modifications, and they efficiently transduce cells to achieve long-term expression of the introduced genes (12). As a result, long-term therapeutic effects may be achieved after a single administration of AAV, as exemplified by the vision-saving gene-replacement therapy (Luxturna) for Leber congenital amaurosis and the life-saving therapies for spinal muscular atrophy (Zolgensma), dopamine-carboxylase deficiency (Upstaza), and others (13). These gene-augmentation therapies require continuous expression of the transgenes to maintain the therapeutic effects. However, such long-term expression of genome editors is potentially dangerous, because it could lead to progressive accumulation of collateral changes in the genome (14, 15). Such changes, which may happen near the target site

* For correspondence: Rafal Hołubowicz, rholubow@uci.edu; Krzysztof Palczewski, kpalczew@uci.edu.

(bystander editing) and in distant genomic loci (off-target editing), even if not detectable during the weeks-to-months timeline of the preclinical genome-editing experiments, could lead to oncogenic or otherwise harmful changes in patient DNA many years after the treatment. Therefore, there is an acute need to develop transient, yet effective genome-editor delivery reagents.

The requirement for transient genome-editor activity in the cell could be satisfied in several alternative ways. The most straightforward approach is direct protein delivery. From the biochemical perspective, this approach seems challenging, as the most commonly used CRISPR-Cas protein Cas9 (from *Streptococcus pyogenes*) is large (158 kDa, Uniprot ID Q99ZW2), and it requires a ∼100 nucleotide-long guide RNA (∼33 kDa) to form a functional RNP (16, 17), which has a substantial net negative charge. Addition of the deaminase or reverse transcriptase enzymes further increases the molecular weight of the RNP, further complicating direct delivery. Nevertheless, the direct administration of RNP, especially when combined with cell-penetrating peptides, has led to promising genome-editing efficiencies, both *in vitro* and *in vivo* (18–22). Liposomes and lipid nanoparticles (LNPs) are capable of increasing the delivery efficiency of the RNP at lower doses, broadening the safety margin (18, 23–25). Alternatively, the protein-coding mRNA may be delivered as an LNP to express the protein *in situ* (26–31). Finally, the desired protein or RNP may be encapsulated within virus-like particles (VLPs). VLPs are a proven vaccine technology (32), and genome-editing VLPs, also known as engineered virus-like particles (eVLPs), nanoblades, engineered delivery vesicles, or engineered nucleocytosolic vehicles for loading of programmable editors (ENVLPEs+), offer an efficient mode of genome-editor delivery (33–40). Translating these basic findings into clinical practice requires scalable manufacturing and purification of VLPs to obtain homogenous, active therapeutic agents that are safe to use in humans. Accordingly, VLP-manufacturing technology has undergone rapid development (41–43). Here, we analyze the limitations of the current state-of-the-art method of VLP purification by direct ultracentrifugation and present an alternative, broadly applicable method of VLP purification by stepwise chromatography. We demonstrate that our method maximizes the specific delivery activity of the VLPs *in vivo*, surpassing the efficiencies observed for VLPs purified by the typical ultracentrifugation procedure. Our VLP-purification process can be applied generally to VLPs encapsulating various protein and RNP cargoes, and it provides a foundation for translation of pure, safe, and effective VLPs.

Results

At a laboratory scale, VLPs are purified using a single-step ultracentrifugation. We found that this procedure may be inadequate for animal studies and hypothesized that the quality of the VLPs may be improved by additional chromatographic steps. We produced eVLPs in human embryonic kidney (HEK) cells after transient transfection with plasmids encoding their components, and we were able to separate the eVLPs from the bulk cell-culture medium by ultracentrifugation through a layer of 20% (w/v) sucrose (Fig. 1*A*). Our eVLPs formed homogenous particles with an approximate diameter of 100 nm, confirming their integrity after ultracentrifugation (Fig. 1*B*). We encapsulated mCherry by fusing it with Gag and tracked the mCherry delivery to HEK cells by fluorescence microscopy (Fig. 1*C*). We detected mCherry in the HEK cells as early as 1 h after application, with peak fluorescence intensity reached around 24 h (Fig. 1, *C* and *D*). To further assess the purification of the eVLPs and expression of their cargo, we encapsulated Cre recombinase as a model genome editor to take advantage of well-established reporter cells and reporter mice. We found that the eVLPs can be manufactured efficiently in cell culture medium with fetal bovine serum (FBS) concentrations as low as 1% (Fig. 1*E*). We employed mass spectrometric analysis, using stable isotope-labeled peptides as internal standards, to quantify specific VLP components: Cre recombinase (Cre), Gag polyprotein, Cas9, tRNA adenosine deaminase (TadA), and reverse transcriptase, and we used label-free LC-MS/MS to determine the origin and abundance of contaminants present in the eVLPs. We found that in the presence of at least 1% FBS, Cre was efficiently encapsulated in the eVLPs (Fig. 1*F*); however, we noted a sharp decrease in production efficiency and purity of the eVLPs made in serum-free Dulbecco's modified Eagle's medium (DMEM) medium. While the eVLPs were produced to higher yield in 10% FBS, label-free quantification revealed that these eVLPs contained a significant amount of serum proteins and intracellular proteins (indicated as "Other") (Fig. 1*G*). The proportion of serum proteins decreased below the detection limit with decreasing concentrations of FBS in the production medium; conversely, the proportion of heat shock, cytoskeletal, ribosomal, and other intracellular proteins increased as the FBS was decreased, which may indicate increased cellular stress and lysis of producer cells with the resulting release of the intracellular material into the cell culture medium. These intracellular proteins were not completely separated from the eVLPs by ultracentrifugation, probably due to nonspecific aggregation on the surface of the eVLPs. All of the tested eVLPs, including those produced in serum-free medium, mediated efficient *loxP* recombination in HEK *loxP*-GFP-red fluorescent protein (RFP) cells (henceforth referred to as "HEK color-switch cells"), as evidenced by GFP to RFP conversion observed by fluorescence microscopy (Fig. 1, *H* and *I*).

Carryover of contaminants due to insufficient single-step purification of the eVLPs, as well as low throughput and poor scalability of the ultracentrifugation procedure, prompted us to develop a more extensive method for purification of the eVLPs *via* chromatography. Moreover, we noted that in most cases, eVLPs purified by a single ultracentrifugation step were retained by centrifugal filters, even with larger 0.45-μm pores. As the starting material, we used eVLPs produced in the presence of 10% FBS, and we took advantage of the large size of the eVLPs to remove bulk protein contaminants from the cell culture media. This initial decontamination was

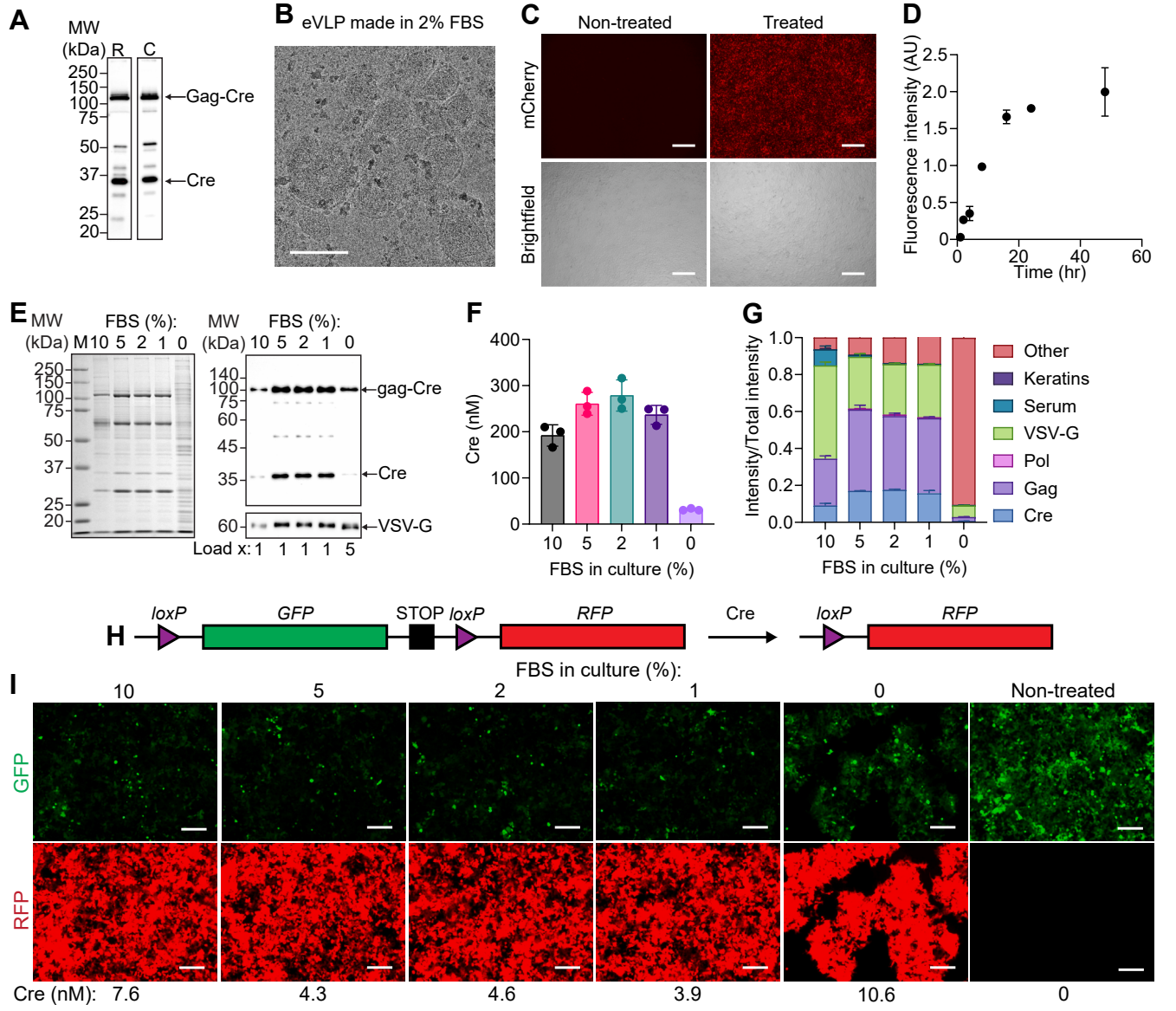

Figure 1. Production and characterization of eVLPs. *A*, representative anti-Cre immunoblots of the Cre-eVLPs before (R) and after (C) purification by sucrose cushion ultracentrifugation. *B*, a representative electron microscopic image of purified eVLPs. Scale bar = 100 nm. *C*, fluorescence-microscopic and brightfield images of HEK 293T cells incubated with mCherry eVLPs for 24 h. Scale bar = 200 μm. *D*, time-course of delivery of mCherry by eVLPs into HEK 293T cells, analyzed by fluorescence microscopy (two biological replicates, mean ± SD). *E*, *left panel*: SDS-PAGE gel images after staining with Coomassie Brilliant Blue of Cre-eVLPs produced in DMEM medium supplemented with 10% (or less) FBS and purified by ultracentrifugation; *upper right panel*: immunoblot of the Cre-eVLPs with anti-Cre antibodies; *lower right panel*: immunoblot of the eVLPs with anti-VSV-G antibodies. The load volume was 0.69 μl of concentrated eVLPs for 1 to 10% FBS and 3.45 μl for 0% FBS. *F*, Quantification of Cre in eVLPs separated by ultracentrifugation (three technical replicates, mean ± SD). *G*, estimation by untargeted mass spectrometry of the relative abundance of classes of proteins in eVLPs (three technical replicates, mean ± SD). *H*, schematic diagram of the genetic construct from the HEK293-loxP-GFP-RFP cells. *I*, delivery of functional Cre recombinase into HEK293-loxP-GFP-RFP cells *via* eVLPs purified by ultracentrifugation. The VLPs were standardized for Gag-Cre by Western blotting. Concentrations of Cre, as measured by SIL peptide quantification, are listed below the images. Scale bar = 200 μm. Shown are representative images of two biological replicates. DMEM, Dulbecco's modified Eagle's medium; eVLP, engineered virus-like particle; FBS, fetal bovine serum; RFP, red fluorescent protein; SIL peptides, stable-isotope-labeled peptides; VSV-G, vesicular stomatitis virus G protein.

accomplished by using Capto Core 400 (CC400) and Capto Core 700 (CC700) resin, which contains an octylamine ligand within the resin particles that binds macromolecules with molecular weights below 700 kDa (Figs. 2, *A* and *B*, S1). We found that CC700 efficiently binds the cell culture proteins with some absorption of eVLPs (Figs. 2*B*, S1*B*, Table S1). The Cre-eVLPs that passed through CC700 retained the ability to mediate *loxP* recombination in the HEK color-switch cells (Fig. 2*C*). We chose adsorption chromatography as a next step to remove remaining contaminants and concentrate the eVLPs after CC700 chromatography. First, we used heparin chromatography due to the known affinity of viruses and VLPs for sulfated glycans (44–46). The elution profile showed the presence of multiple absorbance peaks (Fig. 2*D*), which corresponded to the presence of eVLPs, as evidenced by anti-Cre immunoblots (Fig. 2*E*). We found that a significant

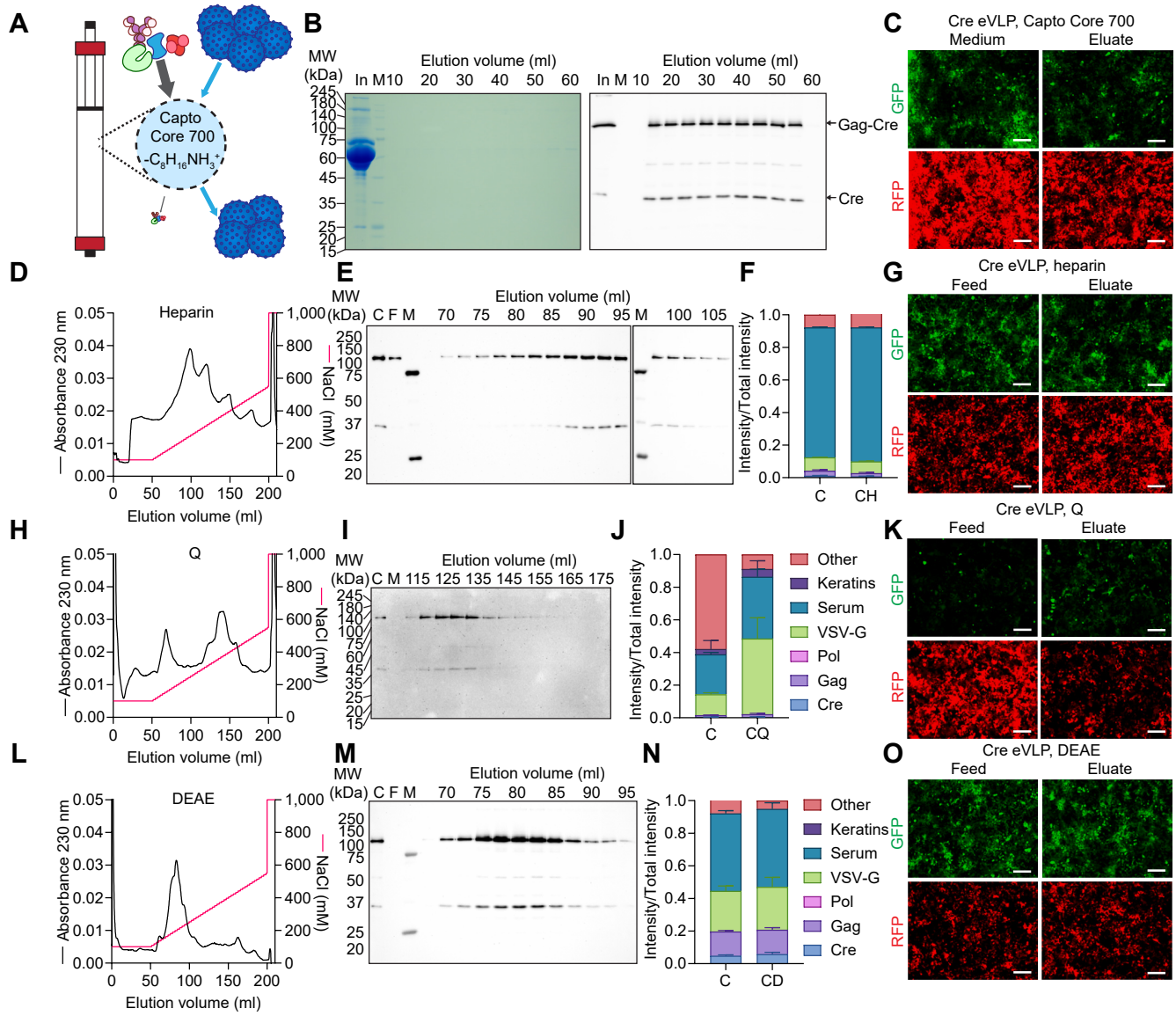

Figure 2. Chromatographic purification of Cre-eVLPs. *A*, schematic diagram of Capto-Core-700 (CC700) chromatography. *B*, Coomassie-stained SDS-PAGE (*left*) and anti-Cre immunoblot (*right*) analyses of Cre-eVLPs, purified by CC700. *C*, conversion of HEK color-switch cells by eVLPs, before (*left*) and after (*right*) CC700-purification. The eVLPs were standardized by immunoblot, and representative images of two biological replicates are shown. Scale bar = 200 μm. *D*, *H*, *L*, comparative chromatograms of Heparin-Sepharose High Performance chromatography (D), Q Sepharose High Performance chromatography (H), and DEAE Sepharose Fast Flow chromatography (L) of eVLPs, prepurified with CC700. *E*, *I*, *M*, comparative anti-Cre Western-blot analyses of fractions collected from the purifications by (E) heparin-, (I) Q-, and (M) DEAE-chromatography. The lane designated "C" contained pooled fractions from CC700 chromatography, and "F" corresponds to a sample of column flowthrough (not shown in the chromatograms). Fractions were loaded at 7.5-fold excess (heparin), 8-fold excess (Q) and 4-fold excess (DEAE) relative to the feed (CC700 pool) and flowthrough. *F*, *J*, *N*, abundance analysis of protein classes detected in eVLPs concentrated on centrifugal filters, before and after purification *via* heparin- (F), Q- (J), or DEAE-chromatography (N); mean ± SD, three technical replicates. *C*, Capto Core 700. *G*, *K*, *O*, conversion of HEK color-switch cells by eVLPs, before (*left*) and after (*right*) further purification *via* heparin- (G), Q- (K), or DEAE-chromatography (O). The contents of the eVLPs were quantified and standardized by anti-Cre immunoblot and SIL mass spectrometry; and ∼1 nM Cre was applied to the cells. Representative images of two biological replicates are shown. Scale bar = 200 μm. In, raw medium; M, protein molecular weight marker; MW, molecular weight; CH, Capto Core 700 and heparin; CQ, Capto Core 700 and Q; CD, Capto Core 700 and DEAE; eVLP, engineered virus-like particle; DEAE, diethylaminoethanol; VSV-G, vesicular stomatitis virus G protein; RPE, retinal pigment epithelium.

fraction of the eVLPs did not bind to the chromatographic resin (Fig. 2*E*, lane "F", Table S1). Proteomic analysis revealed that concentrated Cre-positive fractions contained an increased proportion of serum proteins compared to eVLPs recovered from CC700 (Fig. 2*F*). Nonetheless, heparin chromatography preserved the specific (standardized to Cre) Cre-eVLP delivery activity, despite the low overall yield (56% in flowthrough, 13% in eluate, Fig. 2*G*, Table S1). As an alternative, we processed the eluate from CC700 by anion exchange chromatography on a quaternary amine (Q) resin and found that bound material eluted in two peaks, of which eVLPs were present only in the second peak that was eluted at higher ionic strength, >300 mM NaCl (Fig. 2, *H* and *I*). Notably, when we used a Q-column with a bed volume of 5 ml, a majority of the eVLPs eluted in a total volume of 20 ml, thereby increasing the eVLP concentration relative to

the starting material (typically 60-ml volume). Here, proteomic analysis showed improved purity of the eVLPs (Fig. 2*J*), but the purified Cre-eVLPs had a decreased specific ability to deliver Cre recombinase activity into the HEK color-switch cells (Fig. 2*K*), and the recovery was low (approximately 12%, Table S1). Accordingly, we tried an alternative ion exchanger, diethylaminoethanol (DEAE), and found that it efficiently bound the eVLPs, which were eluted in a major peak early in the gradient with a possible second smaller peak at higher NaCl concentration, >300 mM (Fig. 2, *L* and *M*). Similarly to Q, the eVLPs were concentrated in approximately 20 ml of the DEAE eluate. The recovered eVLPs had a slightly higher purity than the starting material prepurified on CC700 (Fig. 2*N*), and excellent specific Cre-recombinase delivery activity (Fig. 2*O*). Notably, the DEAE chromatography offered the highest recovery of the eVLPs (73%, Table S1).

Comparing multiple batches of Cre-eVLPs purified by single-step ultracentrifugation, we noted significant variability in the properties of the recovered eVLPs. Batch-to-batch, eVLP quality as assessed according to the concentration of Cre (Fig. 3*A*), contamination of the eVLPs (Fig. 3*B*) and Cre-recombinase delivery activity (Fig. S2*A*) varied widely, presenting an obstacle for translational eVLP-delivery studies. The recovery of eVLPs also varied significantly between the runs (Table S1). For example, preparation 47 contained a large proportion of intracellular proteins, and preparation 75 had a very small yield of eVLPs, resulting in peptides being below the limit of quantification *via* LC-MS/MS analysis. To resolve this variability problem, we used chromatographic methods to refine the eVLPs and noted that sequential small-scale CC700 chromatography (Fig. 3*C*) and size-exclusion chromatography (SEC) (Fig. 3*D*) led to progressive removal of contaminating proteins (Fig. 3*E*). In the case of highly contaminated preparation 47, Cre-delivery activity of the eVLPs was preserved (Fig. S2*B*); however, the purity of the final preparation was unacceptable. In the case of preparation 19, which had a significant, but modest, proportion of serum- and cell-derived contaminants, a single SEC step enabled us to obtain a high-purity preparation (Fig. 3*F*). The specific Cre-delivery activity of the resultant eVLPs was slightly decreased in the HEK color-switch assay relative to starting material (Fig. S2*C*). Nevertheless, the high purity of these eVLPs motivated us to evaluate their activity *in vivo*. To this end, we used Cre-reporter mT/mG mice that constitutively express tdTomato. The delivery of Cre recombinase activity leads to excision of a floxed tdTomato-STOP cassette and expression of GFP instead, leading to a color-switch that can be visualized with high precision using two-photon fluorescence microscopy (18, 47–50). Remarkably, in contrast to the *in-vitro*-assay result, the highly purified Cre-eVLPs transduced mouse retinal pigment epithelium (RPE) more efficiently than the crude material (Fig. 3, *G–I*). Our

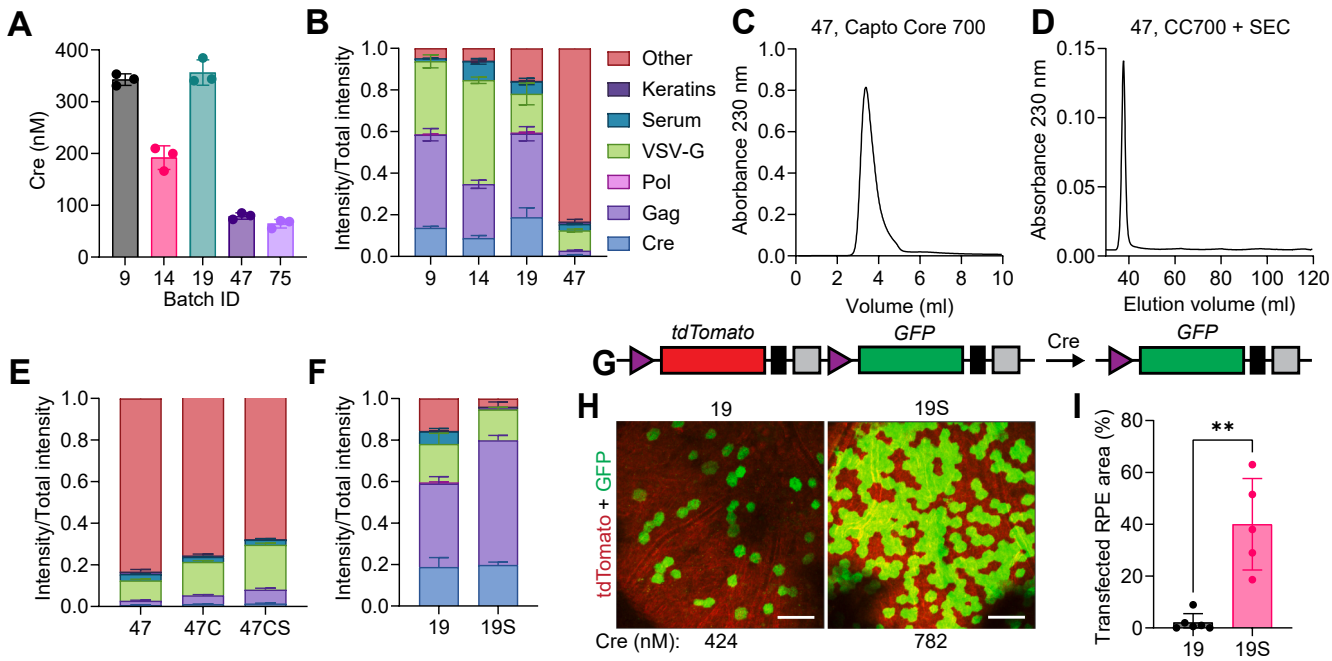

Figure 3. Heterogeneity of Cre eVLPs isolated *via* ultracentrifugation alone. *A*, quantification of Cre in Cre-eVLP preparations purified by ultracentrifugation alone; $n = 3$ technical replicates, mean ± SD. *B*, relative abundance of classes of proteins in eVLPs from $n = 3$ technical replicates, mean ± SD. *C*, chromatogram of eVLP-preparation #47, resolved on a 4.7-ml CC700 column. *D*, chromatogram of eVLP #47 collected from CC700 column, concentrated, then applied and eluted from a HiPrep 16/60 Sephacryl S300HR size-exclusion-chromatography (SEC) column. *E*, classification of detected proteins in eVLP #47 before purification ("47"), after CC700 ("47C"), and after additional SEC chromatography ("47CS"); $n = 3$ technical replicates, mean ± SD. *F*, mass-spectrometric protein identification of eVLP preparation #19 before and after SEC; $n = 3$ replicates, mean ± SD. *G*, schematic diagram of a reporter construct in mT/mG mice. *Purple triangle*, *loxP* site; *black rectangle*, stop cassette; *gray rectangle*, polyadenylation signal. *H*, two-photon tomographic images of intact mT/mG mouse eyes 2 weeks after injection of Cre eVLP #19, before and after SEC purification. Cre concentrations determined *via* SIL mass spectrometry are given below the panels. Scale bar, 100 μm. *I*, quantification of the tdTomato-to-eGFP conversion in the RPE of Cre-eVLP-treated mT/mG mice. Sample size: n = at least five eyes; mean ± SD. Kolmogorov–Smirnov test. **, $p \leq 0.01$. eVLP, engineered virus-like particle; SIL peptides, stable-isotope-labeled peptides.

chromatographic purification method thus maximized *in vivo* activity of the Cre-eVLP.

The excellent recovery of active Cre-eVLPs after DEAE chromatography and the potential for ion-exchange to concentrate the eVLPs prompted us to further develop this approach to purify the eVLPs. We increased the NaCl concentration in the loading buffer from 100 to 125 mM to decrease the binding of contaminants to the DEAE resin and used a steeper NaCl gradient to further concentrate the eluted eVLPs. As expected, the eVLPs prepurified on CC700 still bound efficiently to the DEAE resin at 125 mM NaCl, and a majority of the eVLPs were released from the column in approximately 10 ml of eluate (a ∼2-fold further concentration) (Fig. 4, *A* and *B*). A second peak of eVLPs that eluted later in the gradient became more prominent and appeared to be enriched in surface glycoprotein vesicular stomatitis virus G protein (VSV-G) compared to Cre. In parallel, we performed DEAE chromatography starting from nonpurified production medium and achieved a similar, two-peak elution profile of eVLPs, as shown by immunoblotting (Fig. 4, *C* and *D*). In both cases, the recovery of eVLPs was excellent, up to 100% (Table S1). The SDS-PAGE analysis with silver staining, along with peptide identification *via* LC-MS/MS analysis indicated that DEAE slightly improved the purity of the eVLPs prepurified on CC700 (Figs. 4, *E* and *F*, S3, fractions C and CD). However, serum proteins still comprised most of the collected material, so we used sucrose-cushion ultracentrifugation to further purify the eVLPs (Figs. 4, *E* and *F*, S3, fractions CD and CDS, as well as D and DS). All of the post-DEAE eVLPs displayed Cre-delivery activity with the HEK color-switch cells, but the CC700/DEAE-peak-1 pool appeared to have a somewhat decreased activity (Fig. 4*G*). We then injected the DEAE-purified Cre-eVLPs subretinally into mT/mG mice and found that they had exceptionally high activity *in vivo*. Cre-eVLPs purified on CC700 and DEAE, which contained ∼100 nM Cre (Fig. 4*H*), had greater activity than eVLPs purified by single-step ultracentrifugation at ∼400 nM Cre (Fig. 3*H*). Notably, the eVLPs that were not

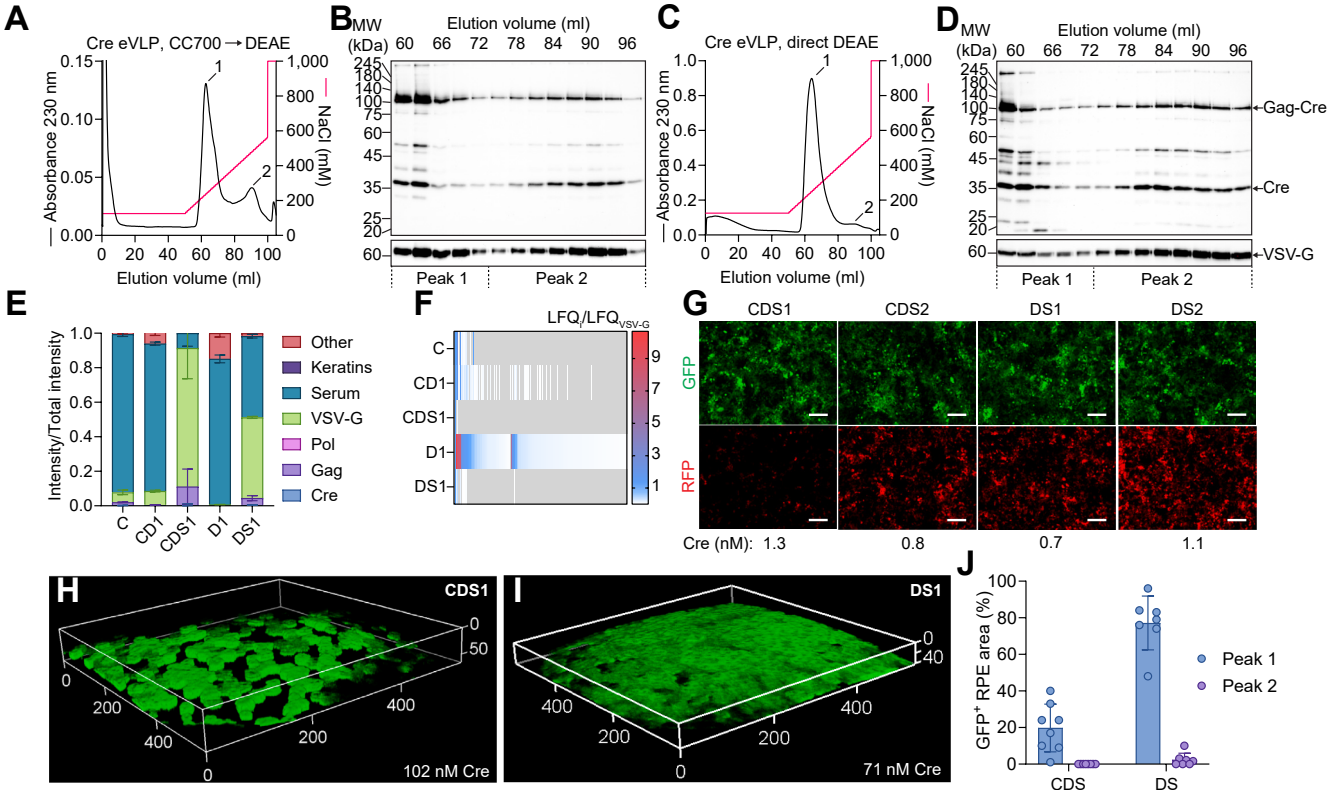

Figure 4. Optimization of ion-exchange chromatographic purification of Cre-eVLPs. *A*, DEAE ion-exchange chromatogram of Cre-eVLPs prepurified on a 20-ml CC700 column, eluted with a steep 10 column-volume (CV) gradient (125–562 mM NaCl). Numbers denote peaks. *B*, anti-Cre (*top*) and anti-VSV-G (*bottom*) immunoblots of fractions of Cre-eVLPs from experiment (A). *C*, DEAE ion-exchange chromatogram of Cre-eVLPs purified directly from the cell culture medium. *D*, anti-Cre (*top*) and anti-VSV-G immunoblots of eVLP fractions from (*C*). *E*, classification of proteins detected in eVLP preparations by untargeted mass spectrometry. *F*, label-free quantification of proteins present in eVLP preparations purified by DEAE and ultracentrifugation (n = 3 technical replicates, mean ± SD). *G*, fluorescence microscopic images of HEK color-switch cells, 48 h after application of Cre-eVLPs, purified *via* DEAE chromatography, and ultracentrifuged. The eVLPs were standardized for Gag-Cre content *via* quantitative immunoblot analysis, and measured concentrations are given below the images. Scale bar = 200 μm. *H*, *I*, two-photon tomographic scans of eyes from mT/mG mice, 6 weeks after subretinal injection of Cre-eVLPs that were purified by DEAE chromatography and ultracentrifugation. Cre concentrations determined *via* SIL mass spectrometry are shown at the *bottom* of the images. Scales represent dimensions in μm. The data are representative of at least seven tomograms. The Cre concentrations are given as means of three technical replicates. *J*, estimation of extent of color conversion in the RPE of the eyes of mT/mG mice treated with purified Cre eVLPs (n = at least 7 eyes, mean ± SD). MW, molecular weight; RPE, retinal pigment epithelium; C, Capto Core 700; CD, Capto Core 700 and DEAE peak 1; CDS, Capto Core 700, DEAE peak 1, and ultracentrifugation; D, direct DEAE peak 1; DS, direct DEAE peak 1, and ultracentrifugation (n = 3 technical replicates, mean ± SD); SIL, stable-isotope-labeled; DEAE, diethylaminoethanol; eVLP, engineered virus-like particle.

prepurified on CC700 had even higher Cre delivery activity *in vivo*, with near complete transduction of the RPE at 71 nM of Cre (Fig. 4, *I* and *J*). This result indicated that direct DEAE ion-exchange chromatography offers excellent extraction of biologically active eVLPs; therefore, we included the DEAE chromatography as a required step in subsequent purification procedures.

Accordingly, we used our prototypical DEAE-purification technique, with and without the CC700 prepurification step, to purify adenine BE (ABE)- and PE-eVLPs programmed to restore the expression of retinoid isomerohydrolase (RPE65) in *rd12* mice, a well-established *in vivo* model of retinal degeneration. The nonsense mutation in exon 3 of *Rpe65* (c.130 C > T; p.R44X) leads to lack of expression of RPE65, no scotopic ERG response, RPE atrophy, and retinal degeneration (51–53). The elution profile of ABE-eVLPs from the DEAE column was identical to that for Cre-eVLPs (Fig. 5, *A–D*), with the exception of an early elution of ABE-eVLPs caused by a technical malfunction of the FPLC system, where high-salt buffer B leaked into the system between system equilibration and the start of the purification of ABE-eVLPs prepurified on CC700 (Fig. 5, *A* and *B*). Immunoblot analysis showed that the ABE-eVLPs were eluted from the DEAE column in two peaks along the NaCl-concentration gradient. Silver staining revealed gradual purification of the eVLPs, especially effective when DEAE was preceded by CC700(Fig. S4, *A* and *B*). LC-MS/MS analysis showed that the pooled eVLPs purified *via* CC700 and DEAE contained serum proteins, which were partly removed upon ultracentrifugation (Fig. 5*E*). The targeted analysis using stable isotope–labeled peptides (SIL peptides) enabled determination of the content of ABE (Cas9 and TadA) and Gag in the eVLPs (Fig. 5*F*). The eVLPs purified directly from the cell culture medium *via* DEAE chromatography had a higher proportion of serum proteins, which were removed by ultracentrifugation (Fig. 5*G*), and encapsulation of ABE was confirmed by SIL peptide-based quantification (Fig. 5*H*). eVLP-mediated ABE delivery was demonstrated in cell culture using *rd12* color-switch cells by induction of GFP fluorescence after correcting the nonsense *Rpe65 rd12* mutation (Fig. 5, *I* and *J*) (18). When injected subretinally into *rd12* mice, both preparations of the ABE-eVLPs (prepurified on CC700 or purified *via* DEAE chromatography alone) led to the rescue of scotopic ERG responses in the *rd12* mice (Fig. 6, *A–C*). The eVLPs purified by DEAE chromatography alone (preparations DS1 and DS2) were especially effective, leading to the appearance

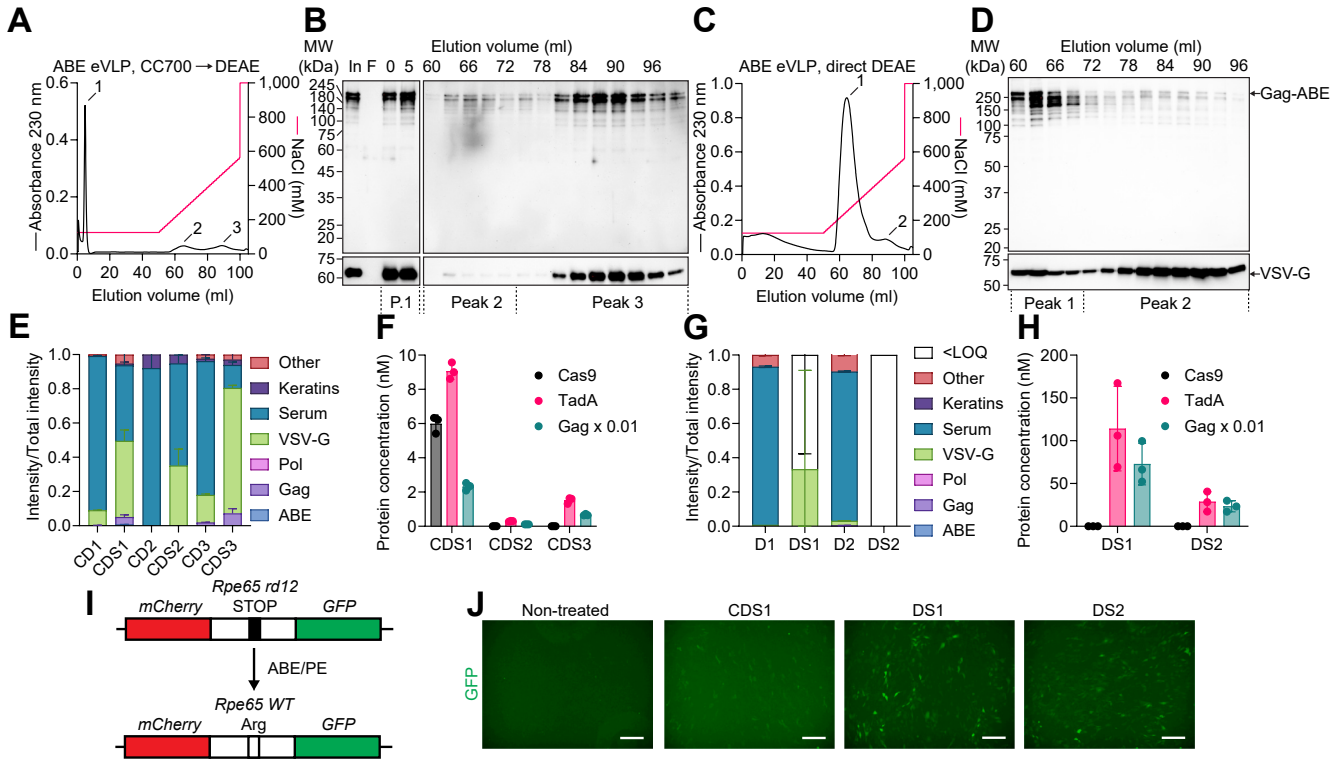

Figure 5. Chromatographic purification of ABE-eVLPs. *A*, DEAE ion-exchange chromatogram of ABE-eVLPs, prepurified on a 20-ml CC700 column. Numbers denote peaks; peak 1 represents early elution caused by leaked buffer B. *B*, anti-Cas9 (*top*) and anti-VSV-G (*bottom*) immunoblots of fractions of ABE-eVLPs from experiment (A). *C*, DEAE ion-exchange chromatogram of ABE-eVLPs, purified directly from the cell culture medium. *D*, anti-Cas9 (*top*) and anti-VSV-G (*bottom*) immunoblots of fractions of ABE-eVLPs from experiment (*C*). *E*,*G*, mass spectrometric classification of proteins detected in purified ABE-eVLPs. Numbers denote peak numbers; S denotes concentration by ultracentrifugation. Three technical replicates, mean ± SD. *F*, *H*, SIL peptide quantification of Cas9, TadA, and Gag in pooled fractions from each peak of DEAE eluate, concentrated by ultracentrifugation. Gag concentrations were divided by 100 for clarity. Three technical replicates, mean ± SD. *I*, schematic cartoon of *rd12* color-switch reporter. *J*, fluorescence microscopic images of *rd12* color-switch reporter cells 48 h after application of purified ABE-eVLPs; scale bar, 200 μm. Representative of two biological replicates. In, CC700 pool; F, flowthrough; MW, molecular weight; CD, ABE-eVLPs, purified by CC700 and DEAE chromatography; D, ABE-eVLPs, purified by DEAE chromatography directly from the medium; "< LOQ", below limit of quantitation; TadA, tRNA adenosine deaminase; SIL peptides, stable-isotope-labeled peptides; ABE, adenine base editing; eVLP, engineered virus-like particle; DEAE, diethylaminoethanol; CC700, Capto Core 700.

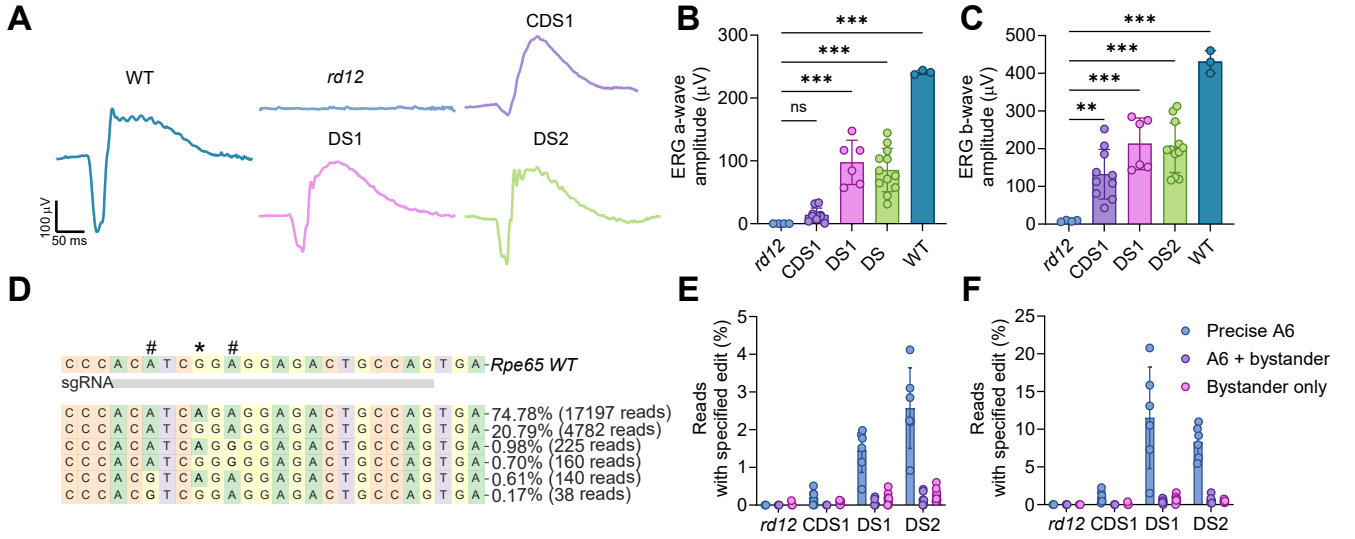

Figure 6. *In vivo* activity of purified ABE-eVLPs. *A*, representative electroretinographic (ERG) traces recorded for *rd12* mice treated with purified ABE-eVLPs. *B,C*, ERG a-wave and b-wave amplitudes recorded for treated *rd12* mice. At least three eyes each were analyzed for wildtype and *rd12* controls; and at least six eyes for treated *rd12* mice; mean ± SD. Ordinary one-way ANOVA with Dunnett's multiple comparisons test. *D*, example of the result of targeted amplicon sequencing analysis done by CRISPResso2. Target adenosine is marked with an *asterisk*; bystander adenosines are marked with *hashes*. The sequences are shown in reverse complement relative to the reading frame of *Rpe65*. *E*, *F*, targeted amplicon sequencing to assess editing efficiency in the *Rpe65 rd12* locus in genomic DNA (D) and cDNA (E), isolated from the RPE of ABE-eVLP-treated *rd12* mice. At least five eyes per treatment group were analyzed, mean ± SD. ABE, adenine base editing; eVLP, engineered virus-like particle; RPE, retinal pigment epithelium.

of ERG responses with prominent a-waves, stimulus-to-b-wave delays similar to those observed for wildtype mice, and ERG waveforms resembling wildtype responses, documenting that healthy function of the retina was achieved in the treated *rd12* mice (Fig. 6*A*). The amplitudes of ERG reached 75% of the values recorded for wildtype mice (Fig. 6, *B* and *C*). On a molecular level (Fig. 6*D*), we found that the precise on-target editing efficiency in the DNA isolated from the RPE and co-isolated choroid and sclera reached 4.1%, with up to 1.0% additional bystander editing (Fig. 6*E*). When we specifically probed *Rpe65* transcripts from the same tissues, which allowed us to focus our analysis on the RPE cells only, we found that restoration of wildtype *Rpe65* reached 20% (Fig. 6*F*). This led to production of the RPE65 protein (Fig. S5*A*) and formation of the visual chromophore, 11-*cis*-retinal, in the treated eyes (Fig. S5*B*). Altogether, these data demonstrate restoration of the critical RPE65 enzymatic activity in the visual cycle, which is absent in the untreated *rd12* mice. The ABE-eVLPs were more efficacious than synthetic ABE-RNP-LNPs (18), as they led to a more pronounced visual response and higher production of 11-*cis* retinoids at a 178-fold lower dose of ABE. Here, the injected dose of TadA was 28 nM, which is equivalent to 14 nM ABE, as there are two TadA subunits per ABE (Fig. 5*H*, sample DS2). The concentration of ABE used in the RNP LNP study was 2500 nM.

We then applied the purification procedures to isolate v3 PE-eVLPs, which offer more versatile and precise editing with minimized risk of bystander editing. DEAE ion exchange chromatography alone or preceded by CC700 chromatography displayed similar copurification of serum proteins. The PE-eVLPs were purified and concentrated in the final ultracentrifugation step (Figs. 7, *A–F*, S6, *A* and *B*). The encapsulation of PE into the eVLPs was less efficient, and the Cas9 was not detectable by immunoblotting of fractions collected during purification nor in the LC-MS/MS analysis. Nevertheless, concentrated PE-eVLPs demonstrated the ability to repair the *Rpe65 rd12* R44X mutation, as reported in the *rd12* color-switch cell assay (Fig. 7*G*). In a similar pattern to the purification of the Cre- and ABE-eVLPs, the PE-eVLPs purified without the CC700 step demonstrated higher activity *in vivo* and led to detectable editing in the *Rpe65 rd12* locus, up to 0.4% in the genomic DNA and up to 0.6% in the cDNA (Fig. 7*H*), along with significant restoration of scotopic vision in the *rd12* mice (Fig. 7*I*).

Motivated by excellent recovery of the biological activity of the eVLPs, we hypothesized that our VLP purification procedure may be applicable to VLPs made on a different scaffold. To demonstrate the broad applicability of our approach, we tested our procedure for isolating next-generation ENVLPEs+, which use HIV-Gag instead of murine leukemia virus (MLV)-Gag, engage a specific aptamer-protein interaction of PP7 with PCP to maximize packaging of functional PE-RNP, and minimize the degradation of prime-editing guide RNA by shielding its 3′ end with Csy4 (33). ENVLPEs+ share a surface glycoprotein VSV-G with the eVLPs but use a different Gag scaffold and are smaller (eVLP – 100–150 nm, ENVLPE+ – 60 nm) (33, 34). We reprogrammed the PE to edit our newly developed tdTomato *in vivo* genome-editing reporter (TIGER) mouse (54) to gain a more detailed insight into the biodistribution of the ENVLPEs+ in the eye. We successfully purified TIGER PE-ENVLPEs+ *via* sequential CC700 and DEAE ion exchange chromatography; however, we noted a significant loss of Cas9 after the CC700

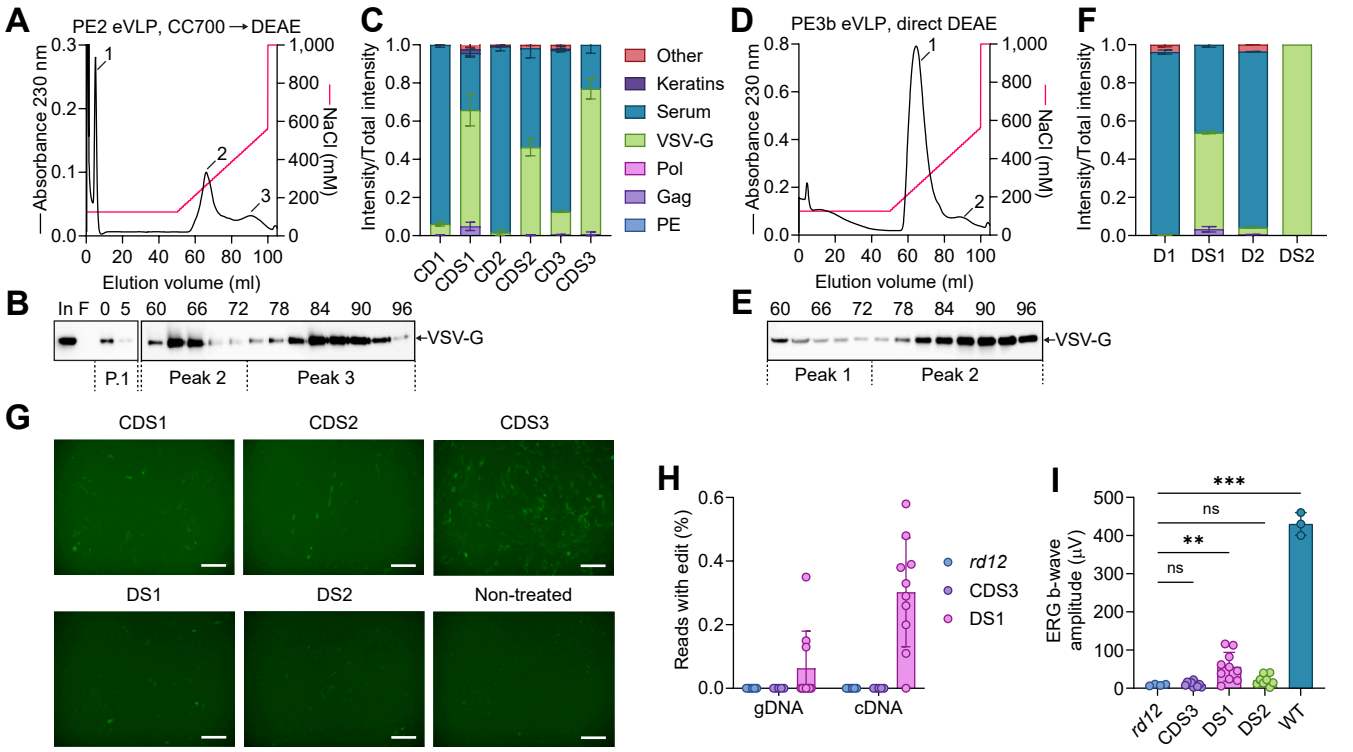

Figure 7. Chromatographic purification of PE-eVLPs. *A*, DEAE ion-exchange chromatogram of PE-eVLPs, prepurified on a 20-ml CC700 column. Numbers denote peaks; peak 1 represents accidental early elution caused by leaked buffer B. *B*, anti-VSV-G immunoblot of fractions of PE-eVLPs from experiment (A). Numbers denote elution volumes. *C*, mass spectrometric classification of proteins detected in purified PE-eVLPs. Numbers correspond to chromatography-peak numbers; S denotes concentration by ultracentrifugation. Three technical replicates, mean ± SD. *D–F*, DEAE ion-exchange chromatogram, anti-VSV-G immunoblot, and mass spectrometric classification of proteins analogous to (*A–C*) for PE-eVLPs, purified directly from the cell-culture medium. *G*, fluorescence microscopic images of *rd12* color-switch reporter cells 48 h after application of purified PE-eVLPs. Scale bar = 200 µm. *H*, targeted amplicon sequencing to document editing efficiency in the *Rpe65 rd12* locus in genomic DNA (gDNA) and cDNA isolated from the RPE of PE-eVLP-treated *rd12* mice. At least five eyes were analyzed per treatment group, mean ± SD. *I*, ERG b-wave amplitudes recorded for treated *rd12* mice. At least three eyes each were analyzed for wildtype and *rd12* controls; at least 10 eyes were analyzed for treated *rd12* mice; mean ± SD. Ordinary one-way ANOVA with Dunnett's multiple comparisons test. ns, $p > 0.05$; **, $p \leq 0.01$; ***, $p \leq 0.001$. In, CC700 pool; F, flowthrough; MW, molecular weight; P, peak; DEAE, diethylaminoethanol; VSV-G, vesicular stomatitis virus G protein; PE, prime editing; eVLP, engineered virus-like particle; CD, PE-eVLP purified by CC700 and DEAE chromatography.

chromatography (Fig. 8*A*), which may be due to removal of unincorporated Cas9 present in the cell culture medium or due to retention of the PE-ENVLPEs+, whose smaller size may make them more prone to absorption by the CC700 (55). The elution profile of PE-ENVLPEs+ from the DEAE column showed two main absorbance peaks, but immunoblot analysis revealed that the first peak may correspond to two species with different relative contents of VSV-G and Cas9 (Fig. 8, *B–E*). The final ultracentrifugation step yielded high-quality PE ENVLPEs+ (Figs. 8*F*, S6, *C* and *D*) that were active in the *in vitro* TIGER reporter-cell assay (Fig. 8*G*) (54). The ENVLPEs+ obtained by direct purification on DEAE were also active *in vivo*, leading to color conversion of approximately 15% of the RPE of treated TIGER mice, at a very low PE concentration of 12 nM (Fig. 8*H*). This latter result demonstrates the exceptional compatibility of direct ion-exchange chromatographic purification with the biological activity of both eVLPs and ENVLPEs+, both of which are biologically active at genome-editor concentrations ≤100 nM, minimizing exposure of the treated tissues to Cas9 and viral proteins, and thus decreasing the risk of adverse reactions.

Discussion

VLPs are effective delivery vehicles for genome editors *in vitro* and *in vivo*. High purity of the VLPs is a prerequisite for clinical translation, with a specific requirement for removal of host cell proteins (HCPs) to less than 100 ng per dose (42). We used electrophoresis with Coomassie Brilliant Blue staining for rapid side-by-side evaluation of the purity of concentrated eVLPs and silver staining to evaluate the progressive purification of the VLPs during chromatography. We gained detailed insights into the protein composition of our VLPs by LC-MS/MS analysis, which enabled us to determine the nature of contaminating proteins and identify molecular species originating from producer cells, cell culture media, or introduced from the environment during the purification. The starting point of our study, single-step ultracentrifugation, efficiently removed serum proteins, but it was unable to deplete HCP, as revealed by LC-MS/MS analysis. We removed these contaminants to some extent by SEC and CC700 chromatography. In our new sequential chromatographic approach, HCPs were present in crude fractions but were removed below the LC-MS/MS-detection limit after the

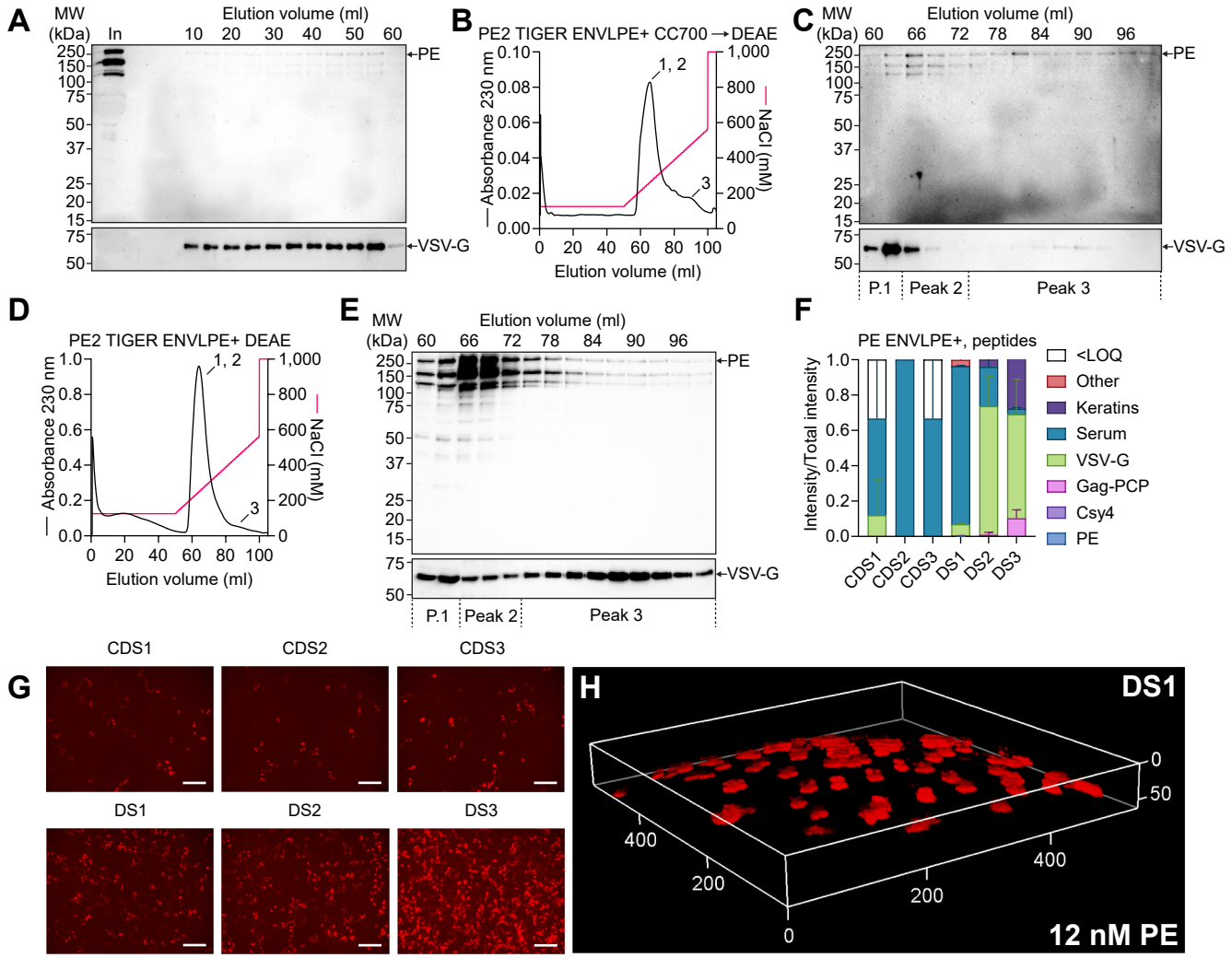

Figure 8. Chromatographic purification of TIGER-converting PE-ENVLPEs+. *A*, anti-Cas9 (*top*) and anti-VSV-G (*bottom*) immunoblots of fractions of PE-ENVLPEs+ collected from a 20-ml CC700 column. *B*, DEAE ion-exchange chromatogram of PE-ENVLPEs+, prepurified on a 20-ml CC700 column; numbers denote absorbance peaks. *C*, anti-Cas9 (top) and anti-VSV-G (bottom) immunoblots of fractions of PE-ENVLPEs+ from experiment (B). *D*,*E*, DEAE ion-exchange chromatogram and immunoblots analogous to (B, C) for PE-ENVLPEs+, purified directly from the cell-culture medium. *F*, mass spectrometric classification of proteins detected in purified PE-ENVLPEs+. Three technical replicates, mean ± SD. *G*, fluorescence microscopic images of TIGER-reporter cells, 48 h after application of purified PE-ENVLPEs+; scale bar = 200 μm. *H*, two-photon fluorescence tomogram of posterior segment of the intact eye of a heterozygous TIGER-reporter mouse treated with PE-ENVLPEs+; scale is in μm. In, filtered production medium; MW, molecular weight; P, peak; CDS1, PE-ENVLPEs + purified by CC700 and DEAE and concentrated by ultracentrifugation; "<LOQ", below limit of quantification; DEAE, diethylaminoethanol; ENVLPE+, engineered nucleocytosolic vehicles for loading of programmable editors; TIGER, tdTomato in vivo genome-editing reporter; PE, prime editing; VSV-G, vesicular stomatitis virus G protein; CC700, Capto Core 700.

final ultracentrifugation. Our results indicate that despite its limited usefulness at the capture step, ultracentrifugation is a preferred final processing step. Production of the VLPs in media with decreased serum concentration may decrease the background of serum proteins, simplify the purification, and improve the economics of VLP production; however, as noted above, decreasing the FBS concentration may induce stress and potentially increase contamination with HCPs.

At present, VLPs are manufactured in transformed cell lines, and as such, are not suitable for pharmaceutical use in humans. Across our samples, we noted that single-step ultracentrifugation resulted in carryover of intracellular proteins such as cytoskeletal proteins, heat shock proteins, histones, and ribosomal proteins, with the histones and ribosomal proteins indicating a possible presence of endogenous nucleic acids. Heat shock proteins and endogenous nucleic acids may be recognized by toll-like receptors as damage-associated molecular patterns, triggering a false tissue damage signal and inducing a necroptotic response in the treated tissue (56–58). This side effect would negate the therapeutic benefit of VLPs. Another class of impurities that is often overlooked in viral and VLP preparations are extracellular vesicles (EVs) (59). The Cre-eVLPs separated by ultracentrifugation and further purified by SEC, which according to LC-MS/MS were the purest in our study (19S, Fig. 3*F*), still contained heat shock cognate 71-kDa protein and CD81, which are markers of EVs (60). The EV-specific proteins were absent in analogous eVLPs purified by DEAE chromatography (Fig. 4, *E* and *F*), which demonstrates the superior resolving power of our stepwise chromatographic purification. We document that highly active

and pure VLPs can be obtained by the combination of chromatography and ultracentrifugation, and we expect that this scalable, broadly applicable ion-exchange capture step will enable the manufacturing of patient-grade genome-editing VLPs on a large scale.

The purification of VLPs presents a unique set of challenges compared to the well-established purification of therapeutic proteins, as exemplified by antibodies. Typically, therapeutic antibodies are expressed in engineered Chinese hamster ovary cells (61) and purified using several filtration and chromatography steps (62). Antibodies are remarkably stable, allowing transient exposure to harsh conditions, such as acidic pH for elution from protein-A affinity-chromatography resin, which is most often used as a first step in their purification. In contrast, VLPs require physiological conditions at all times and maintenance of their mechanical stability (42), which limits the intensity of the chromatographic and filtration techniques that can be used.

To probe the retention of biological activity of the VLPs during purification, we used *in vitro* reporter-cell assays to assess the recombinase activity of Cre and the genome-editing activities of ABE and PE. These fluorescent cell lines are highly sensitive, enable a fast readout, and could be adapted to high-throughput screening. However, they may not reflect potential therapeutic activity accurately, as evidence of high-payload activity in the cell lines is not a guarantee of efficacy *in vivo*, and lack of response *in vitro* does not preclude activity *in vivo*. Our fluorescent reporter cell lines were derived from well-established HEK and 3T3 cell lines, and the sensitivity of the *in vitro* VLP-activity assay was high for HEK cells but low for 3T3 cells, especially considering the very efficient conversion of *rd12*-reporter 3T3-derived cells by ABE- and PE-RNP-Lipofectamine-3000 lipoplexes and RNP-LNPs that we observed previously (18). Nevertheless, our *rd12*-targeting ABE-eVLPs had exceptional activity *in vivo* that outperformed ABE-RNP-LNPs. We reason that naturally evolved cell surface receptor engagement as well as effective mechanisms of virus entry, endosomal escape, and intracellular trafficking enable the eVLPs to direct the ABE activity to its genomic target more efficiently than synthetic LNPs. Moreover, the physiological features of RPE cells, which are specialized for efficient photoreceptor outer segment phagocytosis to maintain the function of the retina, may facilitate the uptake of the VLPs *in vivo* (63). The ability of the RPE to clear material from the subretinal space may explain the efficient genome-editing activity of ABEs encapsulated in protein–lipid VLP vesicles. Therefore, the evidence of effectiveness of VLPs *in vitro* provides a reliable *qualitative* predictor of their utility for delivery to the RPE regardless of the reporter cell line used; however, the extent of the *in vitro* effects is potentially an inaccurate reflection of the *quantitative* dose-response and tissue-specific activity *in vivo*. Induced pluripotent stem cell–derived cell lines and organoids may enable more accurate prediction of the efficacy of tissue-specific and disease-specific VLP therapies (64–71).

The eVLPs and ENVLPEs+ that we used as representative examples had similar surface functionality, originating from the host-cell lipid bilayer and VSV-G surface glycoproteins, but different sizes. The surface properties of our VLPs allowed us to develop a broadly applicable VLP-purification procedure based on ion-exchange chromatography. This broad applicability contrasts with purification of proteins, where the procedures usually need to be customized for each product. The surface of our VSV-G-functionalized VLPs apparently remained similar regardless of the nature of the encapsulated payload or the origin of Gag, while only the size of the VLPs resulted in different behavior during chromatography. Consequently, DEAE chromatography along with a final concentration-purification step of ultracentrifugation will be a useful standard approach for further translational studies of the various VLPs. Compared to single-step ultracentrifugation, DEAE has the advantage of scalability to process large starting volumes and yield product in 2 to 4 column volumes that can be further concentrated with downstream large-scale centrifugation. The excellent recovery of the VLPs from DEAE chromatography—at least 60% compared to less than 20% achievable with heparin and Q (Table S1)—is also a major advantage. Final processing of the VLPs may benefit from further optimization, as the recovery of VLPs after sucrose-cushion ultracentrifugation tends to be low (Table S1). For example, the ultracentrifugation may be done in a sucrose gradient to maintain them in suspension for further automatic fractionation; it would also enhance their monodispersity relative to stressful pelleting. Our method, which maintains mild conditions of low-salt concentration and neutral pH at all steps, leads to excellent recovery of the *in vivo* activity of the encapsulated genome editors. We expect that our VLP-purification procedure using DEAE ion-exchange chromatography could be applied universally, independent of the nature of the protein, RNP, or nucleic acid cargo, thus minimizing the optimization effort needed to tailor the process to each VLP. Depending on the nature of particular VLPs, the purification procedure could be complemented with prepurification on a CC700 column for larger VLPs and Capto Core 400 for smaller VLPs, as summarized in Fig. 9. In future studies, we will increase the scale of purification, streamline the intermediate analytical steps, and further establish our DEAE VLP purification as a method of choice by demonstrating its applicability for VLPs with engineered surface glycoproteins.

Experimental procedures

Mice

All animal experiments were performed in accordance with the ARVO Statement for the Use of Animals in Ophthalmic and Vision Research and with the approved IACUC protocol #AUP-24-073, University of California, Irvine. The mice were maintained on a normal mouse-chow diet and a 12 h/12 h light/dark cycle. The albino mT/mG mice (18, 50), albino TIGER mice (54), *rd12* mice (JAX 005379), and the C57BL/6J mice ('WT', JAX 000664) were housed in the vivarium at the University of California, Irvine. Age and sex of mice are reported in the supporting information.

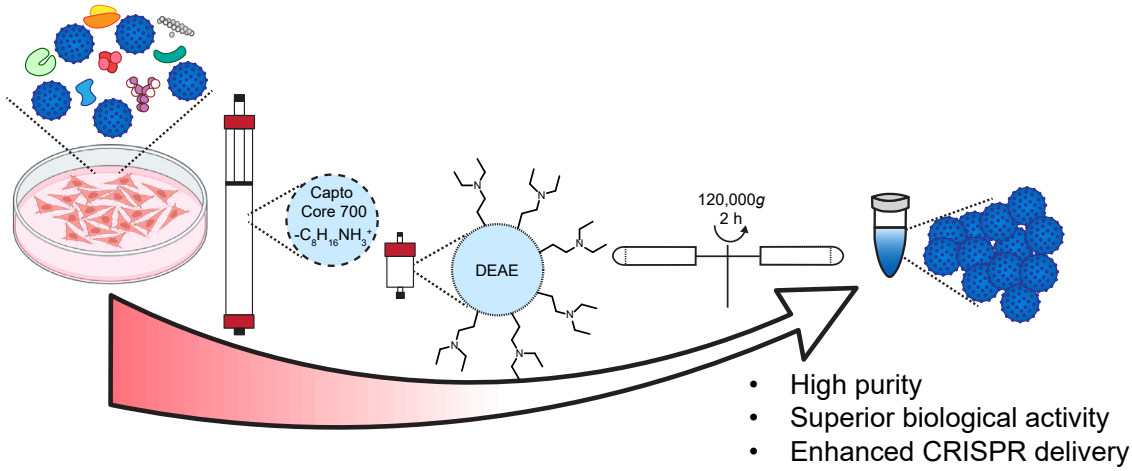

Figure 9. Outline of scalable purification of VLPs. *Left* to *right*: VLPs are produced in mammalian cells and secreted alongside HCP into a culture medium with abundant serum proteins. Sequential steps of Capto Core chromatography, DEAE ion-exchange chromatography, and ultracentrifugation lead to preparation of high-purity VLPs with biological activity and CRISPR delivery potential superior compared to VLPs purified in a single ultracentrifugation step. All the steps can be implemented in good manufacturing practice (GMP) environment and scaled up to manufacture genome-editing VLP therapeutics. DEAE, diethylaminoethanol; HCP, host cell protein; VLP, virus-like particle. Created in part with BioRender.com.

Cell culture

Gesicle-Producer 293T cells (Takara, 632617), HEK 293T/17 cells (Addgene, CRL-11268), HEK293-loxP-GFP-RFP cells (GenTarget Inc., San Diego, SC018-Bsd, referred to as HEK color-switch cells), and TIGER HEK 293T cells (clone 2G7, referred to as TIGER HEK cells) were maintained in DMEM high-glucose medium, plus Glutamax (Thermo Fisher Scientific, 10–569–010) and 10% FBS (Genesee Scientific, 25–514H). The NIH/3T3 *rd12* reporter cell line (referred to as *rd12* color-switch cells) was maintained in DMEM/F12 medium, plus Glutamax (Thermo Fisher Scientific, 10–565–018) and 10% FBS. The cells were cultured in a humidified incubator at 37 °C, 5% CO_2, and passaged using phosphate buffered saline (PBS) pH 7.4 (Thermo Fisher Scientific, 10010023) and 0.05% trypsin with EDTA (Thermo Fisher Scientific, 25300054). The cell lines were not authenticated.

VLP production and collection

Gesicle producer cells were seeded in 100-mm cell culture dishes at a density of 5×10^6 cells per dish. After 20 to 24 h, cells were transfected with a mixture of plasmids encoding eVLP components. For mCherry-, Cre- and ABE-eVLPs, the plasmid mixture contained pCMV-VSV-G (400 ng, Addgene 8454), pBS-CMV-gag-pol (3375 ng, Addgene 35614), MLVgag-cargo plasmid (1125 ng, home-made for Cre and mCherry, Addgene 181753 for ABE), and sgRNA plasmid for ABE (4400 ng). For PE-eVLPs, the plasmids used were pCMV-VSV-G (400 ng), pBS-CMV-gag-pol (2813 ng), gag-MCP-pol (1125 ng, Addgene 211370), gag-PE (563 ng, Addgene 211371), MS2-epegRNA-rd12 (3520 ng), and MS2-ngRNA-rd12 (880 ng). The plasmids were mixed with JetPrime reagent (20 µl) in a total volume of 500 µl of JetPrime buffer, vortexed, incubated at room temperature for 10 min, and applied dropwise onto the cells. The medium was exchanged 24 h after transfection, and the medium with eVLPs was collected 48 h after transfection. Cell seeding and transfection mixtures were doubled for 150-mm dishes. For ENVLPEs+, pCMV-VSV-G plasmid (3200 ng), pCMV ENVLPE+ plasmid (3740 ng, Addgene 232427), pCMV iPE-C P2A Csy4 plasmid (2110 ng, Addgene 232428), and pegRNA PP7 plasmid (10,140 ng, Addgene 232435, modified to target the TIGER construct) were used for transfection with 40 µl of JetPrime in a total volume of 1 ml of JetPrime buffer per 150 mm dish. Guide RNA sequences are reported in Table S3.

The medium was exchanged 24 h after transfection, and the medium with ENVLPEs+ was collected 48 h after transfection. The collected cell culture medium was centrifuged at 500g for 5 min at room temperature to remove aggregates. The supernatant was vacuum filtered through a 0.45-µm PES filter (Genesee Scientific, 25–228). From this point, filtered medium and isolated eVLPs were kept cold on ice or in a cold room (4–8 °C). The filtered medium was subjected to purification *via* chromatography or ultracentrifuged over a 20% (w/v) sucrose cushion in PBS at 120,000*g* for 2 h at 4 °C. The centrifugation was carried out in 28-ml conical tubes (Thermo Fisher Scientific, 75000476) with 20 to 21 ml of medium and 5 ml of 20% (w/v) sucrose in PBS in each of the tubes, which were placed in a SureSpin632 rotor (Thermo Fisher Scientific, 75003031). Pelleted eVLPs were resuspended in buffer A (20 mM Tris-HCl pH 7.4, 100 mM NaCl, 10% (w/v) sucrose, 0.1 mM EDTA). Aggregated VLPs were removed first by centrifugation at 2,000*g* for 5 min at 4 °C and then by filtration through centrifugal filters (Corning Spin-X cellulose acetate: 0.45 µm, cat. 8162; or 0.22 µm, cat. 8160; or Millipore Sigma PVDF Ultrafree 0.5-ml filter, 0.22 µm, cat. UFC30GV0S). Cellulose acetate filters were used for eVLPs, and PVDF filters were used for ENVLPEs+. The filters were prewashed with buffer A at 2,000*g*, 4 °C, for 5 min.

Protein electrophoresis and immunoblotting

The samples were mixed with 4× Laemmli sample buffer (Bio-Rad, 1610747) supplemented with 200 mM DTT

(MilliporeSigma, D9779), then denatured at 75 °C for 10 min, and centrifuged at 17,000*g* for 5 min at room temperature. Hand-cast Tris-glycine-SDS discontinuous polyacrylamide gels with 4% acrylamide in a pH 6.8 stacking gel and 10% acrylamide in a pH 8.8 resolving gel were loaded with the samples and then subjected to a constant voltage of 150 to 180 V, until the bromophenol blue dye migrated to the bottom of the gel.

Coomassie Brilliant Blue staining was done by washing each gel in hot deionized water for 5 min, then placing the gel in Quick Coomassie Stain (Anatrace, GEN-QC-STAIN-1L) and heating the stain and gel in a microwave oven until boiling, followed by gentle mixing on a rocker for at least 1 h. Then, the excess dye was washed out with deionized water, and the gels were placed on a fluorescent light transilluminator and photographed.

The electrophoretically resolved proteins were transferred onto a 0.45-μm PVDF membrane (MilliporeSigma, IPFL00010) with an eBlot L1 apparatus (GenScript), according to the manufacturer's protocol. Then, the membranes were blocked in a mixture of 2.5% nonfat milk in PBS (Cytiva, SH30258.02) with 0.1% Tween 20 (MilliporeSigma, P9416) (PBST) for at least 1 h. The blots were incubated with rabbit anti-Cre polyclonal antibodies (BioLegend 908001, 1:1000–1:5000-dilution, depending on the sample load), mouse anti-VSV-G monoclonal antibodies (MilliporeSigma, V5507, 1:1000–1:10,000), or mouse anti-Cas9 monoclonal antibodies (BioLegend, clone 7A9, cat. 844301, 1:1000) in TBST [10×Tris-buffered saline (Bio-Rad 1706435), diluted to 1× with water and with added 0.1% Tween 20] for at least 1 h. Primary antibodies also contained 0.05% sodium azide (Fisher Scientific, BP922I) as an antimicrobial agent. The blots were washed four times with PBST, at least 5 min at a time, and incubated with goat anti-rabbit horseradish peroxidase (HRP)-linked IgG (Cell Signaling Technology, 7074S, 1:1000–1:5000) or horse anti-mouse HRP-linked IgG (Vector Laboratories, PI-2000–1, 1:10,000) for 1 h. Then, the blots were washed with PBST and developed using SuperSignal West Pico PLUS chemiluminescent substrate (Fisher Scientific, PI34577) or Pierce ECL Plus (Fisher Scientific, 32132). The signal intensities were analyzed in a ChemiDoc MP apparatus (Bio-Rad), using chemiluminescence (Cre, VSV-G, Cas9), or Cy3-and Cy5-fluorescence for prestained protein markers (Bio-Rad 1610374 and Azura Genomics AZ-1141). The concentration and recovery of VLPs were estimated against a serial dilution of batch-specific VLP standard, using ImageLab 6.1.0 software (Bio-Rad).

Cell transduction and imaging

HEK color-switch cells and TIGER HEK cells were seeded at 15,000 cells per well, and *rd12* color-switch cells were seeded at 10,000 cells per well in 96-well plates, approximately 24 h before the experiments. VLPs were diluted to the appropriate concentration with preheated complete culture medium and applied to the cells. The medium was refreshed 24 h after transfection. The cells were imaged at approximately 48 h after transfection in preheated Fluorobrite DMEM medium (Thermo Fisher Scientific, A1896701) with 1% FBS, using an all-in-one Keyence BZ-X810 microscope with GFP or Texas Red (for RFP, mCherry, and tdTomato) optical filters. The time-course analysis was done by applying aliquots of diluted VLPs to the cells at specified time points before imaging. The fluorescence intensity in the images was measured using ImageJ.

Electron microscopy

The suspension of eVLPs was gradually diluted to achieve a sucrose concentration of 0.1% (w/v) in 20 mM Tris pH 7.4, 100 mM NaCl, and 0.1 mM EDTA; then, the eVLPs were concentrated in an Amicon Ultra-4 centrifugal filter device with a 30 kDa molecular weight cut-off (MilliporeSigma, UFC803024). A 5-μl aliquot of purified sample was deposited onto a lacey carbon-film coated grid that was previously glow discharged in a Leica Sputter Coater ACE200 (Leica Microsystems). Excess liquid was blotted for 3.0 s, using a blot force of +8 and 95% humidity at 15 °C, and then rapidly plunged frozen using a Vitrobot Mark IV (Thermo Fisher). The frozen hydrated specimens were then transferred into a Glacios microscope (Thermo Fisher) operated at 200 kV and imaged under low-dose conditions to minimize the radiation damage to the specimen. Images were recorded on a Ceta camera (Thermo Fisher) at a magnification of 36,000×, which has a physical pixel size of 0.4 nm at the specimen space.

Proteomic analysis

Deionized water for all experiments was generated using a Milli-Q water-purification system (Millipore Corporation). Formic acid (FA), ammonium bicarbonate, and acetonitrile of MS grade were purchased from Fisher Chemical. Iodoacetic acid and DTT were of analytical grade and supplied by Millipore Corporation. Sequencing-grade modified trypsin was provided by Promega. SIL peptides were synthesized by GenScript. The stock solutions of all the peptides were prepared by accurately weighing the synthetic peptides and then dissolving them in water, 3% ammonia water (by volume), or DMSO, following the manufacturer's instructions. The SIL peptides (Table S2) were diluted with water before adding them to the samples.

Samples were diluted with 50 mM ammonium bicarbonate and treated with 10 mM DTT for 1 h at 56 °C to reduce disulfides and then with 20 mM iodoacetic acid to alkylate the cysteine residues for 30 min at room temperature in the dark. Then, aliquots of the SIL peptides were added to the protein samples, followed by addition of trypsin at a trypsin-to-protein ratio of 1:50; the reaction mixture was incubated overnight at 37 °C. Trypsin activity was terminated by acidification with 0.1% FA, and the samples were then desalted using a C18 spin column (Thermo Scientific). After drying completely by speed-vacuum, peptides were dissolved in 0.1% FA for LC-MS/MS analysis.

Acquisition of mass-spectrometric data

Samples were analyzed by LC-MS/MS, using a Vanquish HPLC (Thermo Fisher Scientific), coupled in-line with a Q Exactive mass spectrometer (Thermo Fisher Scientific) with an ESI source. Mobile phase A was composed of 0.1% FA in water, and mobile phase B was comprised of 0.1% FA in acetonitrile. The total flow rate was 0.4 ml min^{-1}. Peptides were separated over a 57-min gradient from 4% to 25% buffer B (total run time 90 min per sample) on an Acquity UPLC BEH C18 column (1.7 μm, 2.1 mm × 100 mm, Waters Corporation). The mass spectrometer was operated in a full MS-scan mode (resolution 70,000 at m/z 200) followed by data-dependent MS2 (17,500 resolution), both in the positive mode. The automatic gain control target values were set at 1×10^6 and 1×10^5 for the MS and MS/MS scans, respectively. The maximum injection time was 50 ms for MS and 35 ms for MS/MS. Higher-energy collision dissociation was performed with a stepped-collision energy of 20%, 25%, and 30% with an isolation window of 2.0 Da.

Label-free quantification analysis

The raw LC-MS/MS data files were analyzed using MaxQuant (version 2.6.3.0), with the spectra searched against the UniProt bovine and human proteins (downloaded June 10, 2025); and the proteins encoded on the transfected plasmids. For identification of the peptides, the mass tolerances were 20 ppm for initial precursor ions and 0.5 Da for fragmented ions. Two missed cleavages in tryptic digests were allowed. Cysteine residues were set as static modifications. Oxidation of methionine was set as the variable modification. Filtering for the peptide identification was set at a false discovery rate of 1%. Identified proteins are reported in supporting information.

Targeted analysis

Quantitative data for targeted analysis of Cre, TadA, reverse transcriptase, Cas9, MLV Gag, and HIV Gag were extracted for given precursor ions; and the concentrations were calculated based on the ratio of endogenous peptides and the corresponding SIL peptides (Table S2).

Chromatography

Chromatographic separations were performed in a cold room or in a refrigerated cabinet (4–8 °C). Capto Core chromatography was performed using 4.7-ml CC400 (Cytiva, 17372410) and CC700 (Cytiva 17548115) HiScreen columns, or a 20-ml CC700 resin (Cytiva 17548101) packed into a XK 16/20 column (Cytiva 28988937). The columns were equilibrated with buffer A [20 mM Tris-HCl pH 7.4 (25 °C), 100 mM NaCl, 0.1 mM EDTA, 10% (w/v) sucrose]. VLPs (eVLPs or ENVLPEs+) prepurified by ultracentrifugation were injected into the 4.7-ml CC700 HiScreen column connected to a Bio-Rad DuoFlow FPLC system and resolved at 1.0 ml min^{-1} in buffer A. 0.5-ml fractions were collected and selected for further analysis based on their absorbance at 230 nm. Cell culture medium containing the VLPs was passed through one of the HiScreen columns or through the 20 ml CC700 column at approximately 3.2 ml min^{-1} using a peristaltic pump P-1 (Cytiva 18111091); fractions were collected into round-bottom polypropylene tubes every 1.5 min, using a Gilson FC-203B fraction collector. The unbound material was washed out using buffer A. Collected fractions were analyzed by SDS-PAGE with Coomassie-Blue staining, and the fractions before elution of substantial amounts of contaminating proteins were selected for further purification. CC400 and CC700 columns were regenerated by washing in reverse direction with two column volumes of 2 M NaCl, two column volumes of water, and overnight with 30% isopropanol with 1 M NaOH at a flow rate of 0.15 to 0.30 ml min^{-1}. Then, the columns were washed with water and 20% ethanol for storage.

The VLPs were further purified by heparin chromatography (HiTrap Heparin HP 5 ml, Cytiva 17040703) or ion exchange chromatography (HiTrap Q HP 5 ml, Cytiva 17115401, or HiTrap DEAE FF 5 ml, Cytiva 17515401). The columns were equilibrated with buffer A, which in later experiments had the NaCl concentration increased from 100 to 125 mM. Starting material, corresponding to VLPs prepurified with CC700 or VLPs in cell-culture medium, was passed through each type of column at 0.5 ml min^{-1} using the peristaltic pump. Unbound material was washed out with 5 ml of buffer A, and then each column was connected to the FPLC system and subjected to a 50-ml wash with buffer A, a 150-ml elution with a continuous gradient of 0 to 50% of buffer B (20 mM Tris-HCl pH 7.4 (25 °C), 1 M NaCl, 0.1 mM EDTA, 10% (w/v) sucrose), and then a 25-ml wash with 100% buffer B, all at 0.5 ml min^{-1}. The continuous gradient duration in later experiments was decreased to 50 ml. The volume of fractions collected was 5 ml during the wash, 2.5 ml during the 150-ml gradient, or 1 ml during the 50-ml gradient. The columns were regenerated with 50 ml of 2 M NaCl applied in reverse direction, then washed with water and 20% ethanol for storage.

Size-exclusion chromatography of the eVLPs was accomplished using a HiPrep 16/60 Sephacryl S-300 HR column connected to the FPLC system and equilibrated with buffer A with 100 mM NaCl at 0.4 ml min^{-1}. The suspension of VLPs was injected, and 1-ml fractions were collected; $A_{230\ nm}$ was monitored to identify potential VLP-containing samples, which were further analyzed by immunoblotting against the cargo (Cre, Cas9) and VSV-G.

The verified VLP-containing fractions were concentrated using centrifugal filters appropriate for specific sample volumes (Amicon Ultra 0.5 ml, 4 ml, or 15 ml, molecular weight cut-off 30 kDa, Millipore Sigma UFC503096, UFC803024, or UFC903024, respectively) and centrifuged at 2000*g*, 4 °C. Alternatively, combined purification and concentration of the VLPs was achieved by ultracentrifugation at 120,000*g* for 2 h at 4 °C with at least 1 ml of 20% sucrose cushion in 13.2 ml polypropylene tubes (Beckman Coulter 331372) (SW 41 Ti rotor) or with at least 0.5 ml of 20% sucrose cushion in 2.2 ml polypropylene tubes (Beckman Coulter 347357) (TLS-55 rotor), depending on the sample volume. After

ultracentrifugation, the supernatant was aspirated by vacuum, and the VLPs were resuspended in buffer A and filtered through 0.22-μm filters. Concentration of the VLPs was estimated by immunoblotting against Cre with nonpurified eVLPs as a standard (Cre-eVLPs) or against VSV-G, with VLPs purified using a single-step ultracentrifugation as a standard (ABE- and PE-VLPs). The purified and concentrated VLPs were deemed suitable for *in vivo* experiments after confirmation of Cre, ABE, or PE activity in the appropriate color-switch cells.

Subretinal injection

Subretinal injections were performed as previously described (72). Briefly, the eyes of the mice were bilaterally dilated, first with topical administration of 1% tropicamide ophthalmic solution (Akorn, 17478–102–12), followed by 10% phenylephrine ophthalmic solution (MWI Animal Health, 054243). Mice were then anesthetized by intraperitoneal administration of 20 mg mL^{-1} ketamine and 1.60 mg mL^{-1} xylazine in PBS at a dose of 100 mg kg^{-1} of ketamine and 8 mg kg^{-1} of xylazine. To maintain corneal hydration, a drop of GenTeal Severe Lubricant Eye Gel was applied (0.3% hypromellose, Alcon). Subretinal injections were performed under an ophthalmic surgical microscope (Zeiss). An incision was made using a 27G beveled needle in the cornea proximal to the limbus at the nasal side. A 34G needle with a blunt tip (World Precision Instruments, NF34BL-2), connected to a Nanofil injection holder (World Precision Instruments, NFINHLD) with SilFlex tubing (World Precision Instruments, SILFLEX-2), was inserted through the corneal incision into the anterior chamber and advanced into the subretinal space without touching the lens. Each mouse received a 1-μl injection in each eye at 70 nl s^{-1}, controlled by a UMP3 UltraMicroPump (World Precision Instruments, UMP3-4). After surgery, the mice were placed on a heating pad, and anesthesia was reversed with intraperitoneal 2.5 mg kg^{-1} atipamezole in PBS (MWI Animal Health, 032800).

Two-photon excitation imaging

Two-photon excitation imaging was accomplished using our customized Leica TCS SP8 imaging system with Falcon architecture. The microscope was equipped with spectral detectors and a 1.0 NA 20× water-immersion objective. Excitation light from the Vision S (Coherent) Ti:sapphire laser was tuned to 950 nm. To split signals from GFP and tdTomato, two internal spectral detectors were used with their detection bandwidths set to 490 to 545 nm for GFP and 590 to 680 nm for tdTomato. Intact mouse eyes were imaged *ex vivo*, after euthanasia and enucleation. Leica LAS × 4.7.0.28176 and ImageJ (NIH) were used for the reconstruction of 3D stacks and quantification of transfected cells (47, 48).

Electroretinography

Prior to electroretinography (ERG) recording, mice were dark-adapted for 24 h. Under a safety light, mice were anesthetized by isoflurane inhalation, and their pupils were dilated with topical administration of 1% tropicamide ophthalmic solution and 10% phenylephrine ophthalmic solution, followed by hypromellose (Akorn; 9050–1) for hydration. Each mouse was placed on a heated Diagnosys Celeris rodent-ERG device (Diagnosys LLC). Ocular-stimulator electrodes were placed on the corneas, the reference electrode was positioned subdermally between the ears, and a ground electrode was placed in the rear leg. The eyes were stimulated with a green-light stimulus (peak emission 544 nm, bandwidth ∼160 nm) of −0.3 log (cd s m^{-2}). The responses for 10 stimuli with an interstimulus interval of 10 s were averaged, and the a- and b-wave amplitudes were acquired from the averaged ERG waveform. Data were analyzed with Espion V6 software (Diagnosys LLC).

RPE dissociation, genomic DNA and RNA extraction, and lysate preparation

The mice were sacrificed by CO_2 asphyxiation and secondary cervical dislocation. Mouse eyes were dissected under a light microscope to separate the posterior eyecup (containing RPE, choroid, and sclera) from the retina and anterior segment.

For sequencing analysis, each posterior eyecup was immediately immersed in RLT Plus (Qiagen). RPE, choroid, and scleral cells were detached from the posterior eyecup by gentle pipetting, followed by removal of the remaining posterior eyecup. Cells were then homogenized with QIAshredder (Qiagen, 79654) and processed for genomic DNA and RNA using the AllPrep DNA/RNA Micro kit, according to manufacturer's instructions (Qiagen 80284). The cDNA was prepared using a high-capacity RNA-to-cDNA kit (Applied Biosystems, 4387406), according to the manufacturer's protocol with 9 μl of the prepared RNA as a substrate.

To prepare the protein lysate from the mouse RPE tissue, the dissected posterior eyecup was transferred to a microcentrifuge tube containing 45 μl of ice-cold RIPA buffer (Cell Signaling Technology, 9806S) with protease inhibitors (cOmplete ULTRA EDTA-free, Roche, 05892953001); it was homogenized by vigorous pipetting. The tissue was incubated for 1 h on a rotator in a cold room, briefly centrifuged, and sonicated for 5 s with a 125-W Qsonica sonicator with a microprobe, at a 20% amplitude. The lysate was centrifuged for 20 min at 17,000*g* at 4 °C. The supernatant was denatured with a 4 × -Laemmli sample buffer with added 200 mM DTT at 75 °C for 10 min, and centrifuged at 17,000*g* for 20 min at room temperature. Ten microliters of sample were loaded per well of the discontinuous SDS-PAGE gel, which was then subjected to a constant voltage of 120 V until the bromophenol blue dye migrated to the bottom of the gel. Retinoid isomerase RPE65 was detected by immunoblotting. In-house anti-RPE65 mouse antibodies (73) were diluted 1:1000 in 2.5% milk in TBST with 0.05% sodium azide and applied to the blocked membrane for incubation overnight on a rocker in the cold room. After washing with PBST, the membrane was incubated for 1 h at room temperature on a rocker, with

anti-mouse HRP-conjugated antibodies (Vector Laboratories) diluted 1:2000 in 2.5% milk in TBST, then washed, and developed as described above. The membrane was then thoroughly washed with water and PBST and subsequently probed with anti-β-actin rabbit IgG (Cell Signaling Technology, 4970S) diluted 1:2000 in 2.5% milk in TBST with 0.05% sodium azide and with anti-rabbit HRP-conjugated antibodies (Cell Signaling Technology) diluted 1:5000 in 2.5% milk in TBST for 1 h at room temperature.

Analysis of genome and transcriptome editing

The DNA flanking the *Rpe65 rd12* locus in the genomic DNA and cDNA was amplified using Phusion Plus Green PCR Master Mix (Thermo Fisher Scientific, F632L) and the primers listed in Table S4 (IDT), with initial denaturation at 98 °C for 30 s; 30 cycles of denaturation at 98 °C for 10 s; annealing at 67 °C for 20 s; synthesis at 72 °C for 30 s; and final synthesis at 72 °C for 5 min. PCR1 products were verified on a 2% agarose gel in TAE buffer against a GeneRuler 100-bp DNA ladder (Thermo Fisher Scientific, SM0243). One microliter of PCR1 was used as input for PCR2 to install Illumina barcodes. PCR2 was conducted for 8 to 10 cycles of amplification using Phusion U Multiplex PCR Master Mix (Life Technologies). Following PCR2, samples were pooled and gel-purified on a 1% agarose gel using a QIAquick Gel Extraction Kit (Qiagen). Library concentration was determined using the Qubit High-Sensitivity Assay Kit (Thermo Fisher Scientific). Samples were sequenced on an Illumina MiSeq instrument (single-read, 220–280 cycles) using an Illumina MiSeq v2 300-cycle Kit (Illumina).

Sequencing reads were demultiplexed using the MiSeq Reporter software (Illumina) and were analyzed using CRISPResso2. The reads were qualified for the analysis based on an alignment score of 70 and assigned to distinct alleles (Precise A6, A6 + Bystander, Bystander Only) through the analysis in a quantification window of 20 base pairs centered around a nick site 3 bp upstream of the protospacer-adjacent motif. Editing efficiencies are reported as the percentage of sequencing reads assigned to each allele.

Retinoid analysis

Mice were dark-adapted for 2 days before eye enucleation. Eyes were homogenized in 1 ml of a 10 mM sodium phosphate buffer (pH 8.0) containing 50% methanol (v/v) (Sigma–Aldrich; 34860-1L-R) and 100 mM hydroxylamine, pH 8.0 (Sigma–Aldrich; 159417–100G). After a 15-min incubation at room temperature, 2 ml of 3 M NaCl was added. The resulting sample was extracted twice with 3 ml ethyl acetate (Fisher Scientific; E195–4). Then, the combined organic phase was dried *in vacuo* and reconstituted in 250 µl hexanes. Extracted retinoids (100 µl) were separated on a normal-phase HPLC column (Zorbax Sil; 5 µm; 4.6 mm × 250 mm; Agilent Technologies) connected to an Agilent 1260 Infinity HPLC system equipped with a diode-array detector. Separation was achieved with a mobile phase of 0.6% ethyl acetate in hexanes (Fisher Scientific; H302–4) at a flow rate of 1.4 ml min^{-1} for 17 min, followed by a step increase to 10% ethyl acetate in hexane for an additional 25 min. Retinoids were detected by monitoring absorbance at 325 nm and 360 nm, using Agilent ChemStation software.

Statistical analysis

The graphs were plotted and analyzed using GraphPad Prism 10. Statistical tests were described in figure legends. ns, $p > 0.05$, $^{*}p \le 0.05$; $^{**}p \le 0.01$, $^{***}p \le 0.001$. Full statistical test reports provided by Prism are included in the supporting information.

Data availability—The data underlying this article were deposited in Dryad (https://doi.org/10.5061/dryad.c2fqz61q6). The mass spectrometry proteomics data have been deposited to the ProteomeXchange Consortium *via* the PRIDE (74) partner repository with the dataset identifier PXD070195.

Supporting information—This article contains supporting information.

Acknowledgments—We thank members of the Brunson Center for Translational Vision Research, including Zhiqian Dong, Xiuli Ma, Eleonora Risaliti, Trevor J. Jones, and Natalia G. Opel, for their technical assistance and comments on this work. We thank Dorota Skowronska-Krawczyk (BCTVR) for access to a gel imager and Li Xing (UC Irvine Materials Research Institute) for cryo-EM imaging of the eVLPs.

Author contribution—M. H., P. C., G. P., J. Z., S. D., C. R. M., and R. H. investigation; N. A., J. G., D. L., D.-J. T., and G. W. resources; F. G., G. P., S. D., K. P., C. R. M., D. L., and R. H. writing–original draft; F. G., C. R. M., and R. H. validation; F. G., G. P., C. R. M., and R. H. methodology; F. G. and R. H. formal analysis; F. G., S. D., C. R. M., J. Z., and R. H. data curation. S. D., K. P., and R. H. writing–review & editing; S. D., K. P., D. L., and R. H. funding acquisition. K. P. and R. H. conceptualization; R. H. visualization.

Funding and additional information—R. H. is a Beckman Scholar in Retinal Research and was funded in part by a Career Starter Research Grant and a Career Starter Competitive Renewal Grant from the Knights Templar Eye Foundation. This work was supported in part by grants from the NIH, including R01EY036994 (K. P.), R01EY034501 (K. P.), T32GM008620 (S. W. D.), F30EY033642 (S. W. D.), UG3AI150551 (D. R. L.), U01AI142756 (D. R. L.), R35GM118062 (D. R. L.), and RM1HG009490 (D. R. L.). This work was supported in part by the Howard Hughes Medical Institute (D. R. L.). K. P. and R. H. acknowledge support from the Foundation Fighting Blindness (award number TA-GT-0423–0847-UCI-TRAP and TA-GT-0624-0887-UCI). P. Z. C. is supported by Schmidt Science Fellows, in partnership with the Rhodes Trust, and by a postdoctoral fellowship from the Natural Sciences and Engineering Research Council of Canada. We acknowledge support to the Department of Ophthalmology Gavin Herbert Eye Institute at the University of California, Irvine, from an unrestricted Research to Prevent Blindness award, from NIH core grant P30EY034070, and from a University of California, Irvine School of Medicine Dean's Office grant. This article is subject to HHMI's Open Access to Publications policy. HHMI lab heads have previously granted a nonexclusive CC BY 4.0 license to

Conflicts of interest—K. P. is a consultant for Polgenix Inc. and AbbVie Inc. and serves on the Scientific Advisory Board of Hyperion Eye Ltd. F. G. is partial owner of Lucina Biotherapeutics, Inc. K. P. and G. P. T. are equity holders in Eyesomer Therapeutics. D. R. L. is a consultant and/or equity owner for Prime Medicine, Beam Therapeutics, Pairwise Plants, and nChroma Bio, companies that use or deliver genome-editing or epigenome-engineering agents. All other authors have declared that no conflict of interest exists.

Abbreviations—The abbreviations used are: AAV, adeno-associated virus; ABE, adenine base editing; BE, base editing; CC400, Capto Core 400; CC700, Capto Core 700; DEAE, diethylaminoethanol; EDV, engineered delivery vehicle; EV, extracellular vesicle; eVLP, engineered virus-like particle; ENVLPE+, engineered nucleocytosolic vehicles for loading of programmable editors; ERG, electroretinography; FBS, fetal bovine serum; HCP, host cell protein; HEK, human embryonic kidney cells; LNP, lipid nanoparticle; LOQ, limit of quantitation; MLV, murine leukemia virus; PE, prime editing; Q, quaternary amine; RFP, red fluorescence protein; RNP, ribonucleoprotein; RPE, retinal pigment epithelium; RPE65, retinoid isomerohydrolase; SEC, size-exclusion chromatography; SIL peptides, stable-isotope-labeled peptides; TadA, tRNA adenosine deaminase; TIGER, tdTomato in vivo genome-editing reporter; VLP, virus-like particle; VSV-G, vesicular stomatitis virus G protein.

References

1. Komor, A. C., Kim, Y. B., Packer, M. S., Zuris, J. A., and Liu, D. R. (2016) Programmable editing of a target base in genomic DNA without double-stranded DNA cleavage. *Nature* **533**, 420–424
2. Gaudelli, N. M., Komor, A. C., Rees, H. A., Packer, M. S., Badran, A. H., Bryson, D. I., *et al.* (2017) Programmable base editing of A*T to G*C in genomic DNA without DNA cleavage. *Nature* **551**, 464–471
3. Anzalone, A. V., Randolph, P. B., Davis, J. R., Sousa, A. A., Koblan, L. W., Levy, J. M., *et al.* (2019) Search-and-replace genome editing without double-strand breaks or donor DNA. *Nature* **576**, 149–157
4. Levesque, S., and Bauer, D. E. (2025) CRISPR-based therapeutic genome editing for inherited blood disorders. *Nat. Rev. Drug Discov.* https://doi.org/10.1038/s41573-025-01236-y
5. Musunuru, K., Grandinette, S. A., Wang, X., Hudson, T. R., Briseno, K., Berry, A. M., *et al.* (2025) Patient-specific in vivo gene editing to treat a rare genetic disease. *N. Engl. J. Med.* https://doi.org/10.1056/NEJMoa2504747
6. Sousa, A. A., Terrey, M., Sakai, H. A., Simmons, C. Q., Arystarkhova, E., Morsci, N. S., *et al.* (2025) In vivo prime editing rescues alternating hemiplegia of childhood in mice. *Cell*. https://doi.org/10.1016/j.cell.2025
7. Schindeler, A., Chu, J., Au-Yeung, C., Kao, H. Y., Ginn, S. L., and O'Donohue, A. K. (2025) In vivo precision base editing to rescue mouse models of disease. *Mol. Ther. Nucleic Acids* **36**, 102622
8. Honrath, S., Burger, M., and Leroux, J. C. (2025) Hurdles to healing: overcoming cellular barriers for viral and nonviral gene therapy. *Int. J. Pharm.* **674**, 125470
9. Li, Y., Du, B., Yu, L., Luo, H., Rong, H., Gao, X., *et al.* (2025) Strategies and challenges of cytosolic delivery of proteins. *J. Drug Target* **33**, 837–852
10. Zhang, W., Liu, H., Zhu, B., Li, W., Han, X., Fu, J., *et al.* (2025) Advances in Cytosolic Delivery of Proteins: Approaches, Challenges, and Emerging Technologies. *Chem. Biodivers.* **22**, e202401713
11. van der Koog, L., Gandek, T. B., and Nagelkerke, A. (2022) Liposomes and extracellular vesicles as drug delivery systems: a comparison of composition, pharmacokinetics, and functionalization. *Adv. Healthc. Mater.* **11**, e2100639
12. Bian, X., Zhou, L., Luo, Z., Liu, G., Hang, Z., Li, H., *et al.* (2025) Emerging delivery systems for enabling precision nucleic acid therapeutics. *ACS Nano* **19**, 4039–4083
13. Zhao, Q., Peng, H., Ma, Y., Yuan, H., and Jiang, H. (2025) In vivo applications and toxicities of AAV-based gene therapies in rare diseases. *Orphanet J. Rare Dis.* **20**, 368
14. Park, S. J., Lee, G. E., Cho, S. M., and Choi, E. H. (2025) Recent applications, future perspectives, and limitations of the CRISPR-Cas system. *Mol. Ther. Nucleic Acids* **36**, 102634
15. Kalter, N., Fuster-Garcia, C., Silva, A., Ronco-Diaz, V., Roncelli, S., Turchiano, G., *et al.* (2025) Off-target effects in CRISPR-Cas genome editing for human therapeutics: progress and challenges. *Mol. Ther. Nucleic Acids* **36**, 102636
16. Jinek, M., Chylinski, K., Fonfara, I., Hauer, M., Doudna, J. A., and Charpentier, E. (2012) A programmable Dual-RNA-Guided DNA endonuclease in adaptive bacterial immunity. *Science* **337**, 816–821
17. Hsu, P. D., Scott, D. A., Weinstein, J. A., Ran, F. A., Konermann, S., Agarwala, V., *et al.* (2013) DNA targeting specificity of RNA-guided Cas9 nucleases. *Nat. Biotechnol.* **31**, 827
18. Holubowicz, R., Du, S. W., Felgner, J., Smidak, R., Choi, E. H., Palczewska, G., *et al.* (2025) Safer and efficient base editing and prime editing via ribonucleoproteins delivered through optimized lipid-nanoparticle formulations. *Nat. Biomed. Eng.* **9**, 57–78
19. Foss, D. V., Muldoon, J. J., Nguyen, D. N., Carr, D., Sahu, S. U., Hunsinger, J. M., *et al.* (2023) Peptide-mediated delivery of CRISPR enzymes for the efficient editing of primary human lymphocytes. *Nat. Biomed. Eng.* **7**, 647–660
20. Zhang, Z., Baxter, A. E., Ren, D., Qin, K., Chen, Z., Collins, S. M., *et al.* (2024) Efficient engineering of human and mouse primary cells using peptide-assisted genome editing. *Nat. Biotechnol.* **42**, 305–315
21. Sahu, S. U., Castro, M., Muldoon, J. J., Asija, K., Wyman, S. K., Krishnappa, N., *et al.* (2025) Peptide-enabled ribonucleoprotein delivery for CRISPR engineering (PERC) in primary human immune cells and hematopoietic stem cells. *Nat. Protoc.* https://doi.org/10.1038/s41596-025-01154-8
22. Kulhankova, K., Traore, S., Cheng, X., Benk-Fortin, H., Hallee, S., Harvey, M., *et al.* (2023) Shuttle peptide delivers base editor RNPs to rhesus monkey airway epithelial cells in vivo. *Nat. Commun.* **14**, 8051
23. Chen, K., Han, H. S., Zhao, S., Xu, B. Y., Yin, B. Y., Lawanprasert, A., *et al.* (2024) Lung and liver editing by lipid nanoparticle delivery of a stable CRISPR-Cas9 ribonucleoprotein. *Nat. Biotechnol.* https://doi.org/10.1038/s41587-024-02437-3
24. Wei, T., Cheng, Q., Min, Y. L., Olson, E. N., and Siegwart, D. J. (2020) Systemic nanoparticle delivery of CRISPR-Cas9 ribonucleoproteins for effective tissue specific genome editing. *Nat. Commun.* **11**, 3232
25. Suzuki, Y., Onuma, H., Sato, R., Sato, Y., Hashiba, A., Maeki, M., *et al.* (2021) Lipid nanoparticles loaded with ribonucleoprotein-oligonucleotide complexes synthesized using a microfluidic device exhibit robust genome editing and hepatitis B virus inhibition. *J. Control. Release* **330**, 61–71
26. Kim, M., Song, E. S., Chen, J. C., Chatterjee, S., Sun, Y., Lee, S. M., *et al.* (2025) Dual SORT LNPs for multi-organ base editing. *Nat. Biotechnol.* https://doi.org/10.1038/s41587-025-02675-z
27. Xue, Y. E., Wang, C., Li, H. Y., Du, S., Zhong, Y. C., Zhang, Y. B., *et al.* (2025) Lipid nanoparticles enhance mRNA delivery to the central nervous System upon intrathecal injection. *Adv. Mat.* **37**, e2417097
28. Masarwy, R., Breier, D., Stotsky-Oterin, L., Ad-El, N., Qassem, S., Naidu, G. S., *et al.* (2025) Targeted CRISPR/Cas9 lipid nanoparticles elicits therapeutic genome editing in head and neck cancer. *Adv. Sci. (Weinh)* **12**, e2411032

29. Rothgangl, T., Talas, A., Ioannidi, E. I., Weber, Y., Bock, D., Matsushita, M., *et al.* (2025) Treatment of a metabolic liver disease in mice with a transient prime editing approach. *Nat. Biomed. Eng.* https://doi.org/10.1038/s41551-025-01399-4
30. Mao, K., Tan, H., Cong, X., Liu, J., Xin, Y., Wang, J., *et al.* (2025) Optimized lipid nanoparticles enable effective CRISPR/Cas9-mediated gene editing in dendritic cells for enhanced immunotherapy. *Acta Pharm. Sin B* **15**, 642–656
31. Degtev, D., Bravo, J., Emmanouilidi, A., Zdravkovic, A., Choong, O. K., Liz Touza, J., *et al.* (2024) Engineered PsCas9 enables therapeutic genome editing in mouse liver with lipid nanoparticles. *Nat. Commun.* **15**, 9173
32. Nooraei, S., Bahrulolum, H., Hoseini, Z. S., Katalani, C., Hajizade, A., Easton, A. J., *et al.* (2021) Virus-like particles: preparation, immunogenicity and their roles as nanovaccines and drug nanocarriers. *J. Nanobiotechnology* **19**, 59
33. Geilenkeuser, J., Armbrust, N., Steinmassl, E., Du, S. W., Schmidt, S., Binder, E. M. H., *et al.* (2025) Engineered nucleocytosolic vehicles for loading of programmable. *Cell* **188**, 2637–2655.e2631
34. Banskota, S., Raguram, A., Suh, S., Du, S. W., Davis, J. R., Choi, E. H., *et al.* (2022) Engineered virus-like particles for efficient in vivo delivery of therapeutic proteins. *Cell* **185**, 250–265.e216
35. An, M., Raguram, A., Du, S. W., Banskota, S., Davis, J. R., Newby, G. A., *et al.* (2024) Engineered virus-like particles for transient delivery of prime editor ribonucleoprotein complexes in vivo. *Nat. Biotechnol.* **42**, 1526–1537
36. Kaczmarczyk, S. J., Sitaraman, K., Young, H. A., Hughes, S. H., and Chatterjee, D. K. (2011) Protein delivery using engineered virus-like particles. *Proc. Natl. Acad. Sci. U.S.A.* **108**, 16998–17003
37. Montagna, C., Petris, G., Casini, A., Maule, G., Franceschini, G. M., Zanella, I., *et al.* (2018) VSV-G-Enveloped vesicles for traceless delivery of CRISPR-Cas9. *Mol. Ther. Nucleic Acids* **12**, 453–462
38. Mangeot, P. E., Risson, V., Fusil, F., Marnef, A., Laurent, E., Blin, J., *et al.* (2019) Genome editing in primary cells and in vivo using viral-derived Nanoblades loaded with Cas9-sgRNA ribonucleoproteins. *Nat. Commun.* **10**, 45
39. Hamilton, J. R., Chen, E., Perez, B. S., Sandoval Espinoza, C. R., Kang, M. H., Trinidad, M., *et al.* (2024) In vivo human T cell engineering with enveloped delivery vehicles. *Nat. Biotechnol.* **42**, 1684–1692
40. Halegua, T., Risson, V., Carras, J., Rouyer, M., Coudert, L., Jacquier, A., *et al.* (2025) Delivery of prime editing in human stem cells using pseudoviral NanoScribes particles. *Nat. Commun.* **16**, 397
41. Zhao, L., and Ma, G. (2025) Chromatography media and purification processes for complex and super-large biomolecules: a review. *J. Chromatogr. A* **1744**, 465721
42. Gashti, A. B., Patel, M., Chahal, P. S., Hrapovic, S., Gilbert, R., Morasse, A., *et al.* (2025) Purification and functional characterization of gag-spike virus-like particles: process optimization for efficient vaccine production. *Vaccine* **62**, 127500
43. Park, E. Y., and Minkner, R. (2025) A systematic approach for scalable purification of virus-like particles. *Protein Expr. Purif.* **228**, 106664
44. Joyce, J. G., Tung, J. S., Przysiecki, C. T., Cook, J. C., Lehman, E. D., Sands, J. A., *et al.* (1999) The L1 major capsid protein of human papillomavirus type 11 recombinant virus-like particles interacts with heparin and cell-surface glycosaminoglycans on human keratinocytes. *J. Biol. Chem.* **274**, 5810–5822
45. Cheng, F., Tsvetkova, I. B., Khuong, Y. L., Moore, A. W., Arnold, R. J., Goicochea, N. L., *et al.* (2013) The packaging of different cargo into enveloped viral nanoparticles. *Mol. Pharmaceut.* **10**, 51–58
46. Zollner, A. M., Ruiz, L. G., Mayer, V., Stohl, S., Jakob, L. A., Lingg, N., *et al.* (2024) Heparin-affinity chromatography is a generic purification platform for chimeric gag VLPs displaying different viral surface antigens. *Sep. Purif. Technol.* **340**
47. Palczewska, G., Boguslawski, J., Stremplewski, P., Kornaszewski, L., Zhang, J., Dong, Z., *et al.* (2020) Noninvasive two-photon optical biopsy of retinal fluorophores. *Proc. Natl. Acad. Sci. U.S.A.* **117**, 22532–22543
48. Palczewska, G., Dong, Z., Golczak, M., Hunter, J. J., Williams, D. R., Alexander, N. S., *et al.* (2014) Noninvasive two-photon microscopy imaging of mouse retina and retinal pigment epithelium through the pupil of the eye. *Nat. Med.* **20**, 785–789
49. Maeda, A., Palczewska, G., Golczak, M., Kohno, H., Dong, Z., Maeda, T., *et al.* (2014) Two-photon microscopy reveals early rod photoreceptor cell damage in light-exposed mutant mice. *Proc. Natl. Acad. Sci. U.S.A.* **111**, E1428–E1437
50. Muzumdar, M. D., Tasic, B., Miyamichi, K., Li, L., and Luo, L. (2007) A global double-fluorescent Cre reporter mouse. *Genesis* **45**, 593–605
51. Pang, J. J., Chang, B., Hawes, N. L., Hurd, R. E., Davisson, M. T., Li, J., *et al.* (2005) Retinal degeneration 12 (rd12): a new, spontaneously arising mouse model for human Leber congenital amaurosis (LCA). *Mol. Vis.* **11**, 152–162
52. Choi, E. H., Suh, S., Foik, A. T., Leinonen, H., Newby, G. A., Gao, X. D., *et al.* (2022) In vivo base editing rescues cone photoreceptors in a mouse model of early-onset inherited retinal degeneration. *Nat. Commun.* **13**, 1830
53. Suh, S., Choi, E. H., Leinonen, H., Foik, A. T., Newby, G. A., Yeh, W. H., *et al.* (2021) Restoration of visual function in adult mice with an inherited retinal disease via adenine base editing. *Nat. Biomed. Eng.* **5**, 169–178
54. Du, S. W., Palczewska, G., Dong, Z., Lauterborn, J. C., Kaipa, B. R., Yan, A. L., *et al.* (2025) TIGER: a tdTomato in-vivo genome-editing reporter mouse for investigating precision-editor delivery approaches. *P Natl. Acad. Sci. U.S.A.* **122**, e2506257122
55. Mi, X., Wang, S. C., Winters, M. A., and Carta, G. (2023) Protein adsorption on core-shell resins for flow-through purifications: Effect of protein molecular size, shape, and salt concentration. *Biotechnol. Progr.* **39**, e3300
56. Behzadi, P., García-Perdomo, H. A., and Karpinski, T. M. (2021) Toll-like receptors: general molecular and structural biology. *J. Immunol. Res.* **2021**, 9914854
57. Meier, P., Legrand, A. J., Adam, D., and Silke, J. (2024) Immunogenic cell death in cancer: targeting necroptosis to induce antitumour immunity. *Nat. Rev. Cancer* **24**, 299–315
58. Mahaling, B., Low, S. W. Y., Beck, M., Kumar, D., Ahmed, S., Connor, T. B., *et al.* (2022) Damage-associated molecular patterns (DAMPs) in retinal disorders. *Int. J. Mol. Sci.* **23**, 2591
59. Fernandes, C., Persaud, A. T., Chaphekhar, D., Burnie, J., Belanger, C., Tang, V. A., *et al.* (2025) Flow virometry: recent advancements, best practices, and future frontiers. *J. Virol.* **99**, e0171724
60. Fan, Y., Pionneau, C., Cocozza, F., Boëlle, P. Y., Chardonnet, S., Charrin, S., *et al.* (2023) Differential proteomics argues against a general role for CD9, CD81 or CD63 in the sorting of proteins into extracellular vesicles. *J. Extracell Vesicles* **12**, e12352
61. Dahodwala, H., and Sharfstein, S. T. (2017) The 'omics revolution in CHO biology: roadmap to improved CHO productivity. *Methods Mol. Biol.* **1603**, 153–168
62. Chahar, D. S., Ravindran, S., and Pisal, S. S. (2020) Monoclonal antibody purification and its progression to commercial scale. *Biologicals* **63**, 1–13
63. Lakkaraju, A., Umapathy, A., Tan, L. X., Daniele, L., Philp, N. J., Boesze-Battaglia, K., *et al.* (2020) The cell biology of the retinal pigment epithelium. *Prog. Retin. Eye Res.* https://doi.org/10.1016/j.preteyeres.2020.100846100846
64. Piccolo, D., Sladen, P., Guarascio, R., Ziaka, K., and Cheetham, M. E. (2025) Investigation of ABCA4 missense variants and potential small molecule rescue in retinal organoids. *Invest. Ophthalmol. Vis. Sci.* **66**, 58
65. Li, Y., Yang, R. R., Li, Y. S., Hsu, C. W., Jenny, L. A., Kong, Y., *et al.* (2024) Evaluating precision medicine approaches for gene therapy in patient-specific cellular models of bietti crystalline dystrophy. *JCI Insight* **9**, e177231
66. Maeda, T., and Takahashi, M. (2023) iPSC-RPE in retinal degeneration: recent advancements and future perspectives. *CSH Perspect. Med.* **13**, a041308
67. Watson, A., and Lako, M. (2023) Retinal organoids provide unique insights into molecular signatures of inherited retinal disease throughout retinogenesis. *J. Anat.* **243**, 186–203

68. Suleman, S., Alhaque, S., Guo, A. D., Zhang, A. R., Fawaz, S., Perera, S., *et al.* (2025) Transcriptomic profiling of iPS cell-derived hepatocyte-like cells reveals their close similarity to primary liver hepatocytes. *Cells* **14**, 925
69. Klompstra, T. M., Yoon, K. J., and Koo, B. K. (2025) Evolution of organoid genetics. *Eur. J. Cell Biol.* **104**, 151481
70. Daoud, A., Xia, S., Laselva, O., Jiang, J., and Bear, C. E. (2025) Testing organ-specific responses to therapies in tissues differentiated from cystic fibrosis patient derived iPSCs. *Stem Cell Res.* **83**, 103653
71. Generali, M., Kehl, D., Meier, D., Zorndt, D., Atrott, K., Saito, H., *et al.* (2025) Generation and purification of iPSC-derived cardiomyocytes for clinical applications. *Stem Cell Res. Ther.* **16**, 189
72. Du, S. W., Newby, G. A., Salom, D., Gao, F., Menezes, C. R., Suh, S., *et al.* (2024) In vivo photoreceptor base editing ameliorates rhodopsin-E150K autosomal-recessive retinitis pigmentosa in mice. *Proc. Natl. Acad. Sci. U.S.A.* **121**, e2416827121
73. Golczak, M., Kiser, P. D., Lodowski, D. T., Maeda, A., and Palczewski, K. (2010) Importance of membrane structural integrity for RPE65 retinoid isomerization activity. *J. Biol. Chem.* **285**, 9667–9682
74. Perez-Riverol, Y., Bandla, C., Kundu, D. J., Kamatchinathan, S., Bai, J. W., Hewapathirana, S., *et al.* (2024) The PRIDE database at 20 years: 2025 update. *Nucleic Acids Res.* **53**, D543–D553